Journal of Medicinal Chemistry

ARTICLE

pubs.acs.org/jmc

N-Fused Imidazoles As Novel Anticancer Agents That Inhibit Catalytic Activity of Topoisomerase IIα and Induce Apoptosis in G1/S Phase

Ashish T. Baviskar,[†] Chetna Madaan,[†] Ranjan Preet,[‡] Purusottam Mohapatra,[‡] Vaibhav Jain,[†] Amit Agarwal,[†] Sankar K. Guchhait,[*,†] Chanakya N. Kundu,[*,‡] Uttam C. Banerjee,[†] and Prasad V. Bharatam[†]

[†]National Institute of Pharmaceutical Education and Research (NIPER), Sector 67, SAS Nagar (Mohali), Punjab-160062, India

[‡]School of Biotechnology, KIIT University, Campus-11, Patia, Bhubaneswar, Orissa-751024, India

Supporting Information

ABSTRACT: On the basis of structures of known topoisomerase II catalytic inhibitors and initial molecular docking studies, bicyclic N-fused aminoimidazoles were predicted as potential topoisomerase II inihibitors. They were synthesized by multicomponent reactions and evaluated against human topoisomerase IIα (hTopoIIα) in decatenation, relaxation, cleavage complex, and DNA intercalation in vitro assays. Among 31 compounds of eight different bicyclic scaffolds, it was found that imidazopyridine, imidazopyrazole, and imidazopyrazine with suitable substituents exhibited potent inhibition of catalytic activity of hTopoIIα while not showing DNA intercalation. Molecular docking studies and molecular dynamics (MD) simulation analysis, ATPase-kinetics and ATP-dependent plasmid relaxation assay revealed the catalytic mode of inhibition of the title compounds plausibly by blocking the ATP-binding site. N-Fused aminoimidazoles showed potent anticancer activities in kidney and breast cancer cell lines, low toxicity to normal cells, relatively higher potency compared to etoposide and 5-fluorouracil in kidney cancer cell lines, and potent inhibition in cell migration. These compounds were found to exert apoptotic effect in G1/S phase.

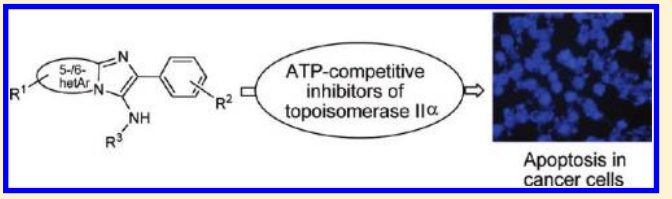

INTRODUCTION

DNA topoisomerase (topo) has been recognized as an important target in anticancer drug discovery.[1−5] About 50% of antitumoral treatment regimens rely on the use of at least one drug that inhibits topoisomerases.[6,7] Several clinically important antitumoral drugs such as doxorubicin and daunorubicin (anthracycline class), etoposide and teniposide (epipodophyllotoxin class), mitoxanthrone, amonafide, and amsacrine target the type II topoisomerase.[8,9] Camptothecin, a clinically important antitumoral drug, and its derivatives target the type I topoisomerase.[10,11] The development of dual topoisomerase I and II inhibitors as anticancer drugs is also recently emerging.[12]

Topoisomerases (I and II) are essential nuclear enzymes that maintain the topological changes of DNA and play key role in transcription, replication, and chromosome segregation.[13−16] Topoisomerase I catalyzes the relaxation of superhelical DNA by transiently making a break in the single strand and allowing either controlled rotation of the double helix about the nick or passage of other strand through the nick before resealing it.[17,18] The topoisomerase II creates double-stranded DNA breaks in concert and allow the passage of a second double-stranded DNA through the transiently broken duplex.[19] Human topoisomerase II exists in two isoforms, α (alpha) and β (beta). While the β isozyme expression remains relatively constant and at relatively low level throughout the cell cycle, α isozyme increases its expression throughout S phase and peaks with 2−3-fold at G2/M phase of mitosis and its concentration is even higher in rapidly proliferating tissues than in quiescent cell populations.[20−22] However, the enzymological differences between topoisomerase IIα and β are subtle and a little is known about the physiological role of β-isoform.[23,24]

Drugs or agents acting on topoisomerase II based on their mode of action are classified into two: topoisomerase II poison and topoisomerase II catalytic inhibitor.[25] Topoisomerase II poisons stabilize the cleavable complex of topoisomerase II with DNA by forming the covalent ternary complex of drug/agent-cleaved G segment DNA−topo II, thus block religation, and enzyme release and induce apoptosis. Topoisomerase II catalytic inhibitors act at any of the other steps of catalytic cycle than the poisons do. Several topo II poisons such as doxorubicin, etoposide, amsacrine, mitoxantrone, and ellipticine are currently widely used in clinical treatment of cancer. However, despite their importance in cancer chemotherapy, considerable evidence indicates that topoisomerase II poisons, related to the level of enzyme-associated DNA breaks versus recombination-repair pathways for induction of apoptosis, may trigger chromosomal translocations that lead to specific leukemias.[26,27] Thus, in recent years, the development of topo II catalytic inhibitors modulating the cytotoxic effects of topo II poisons and overcoming the multidrug resistance (MDR) has gained importance.[28−30] Topoisomerase II catalytic inhibitors are

Received: March 1, 2011
Published: June 06, 2011

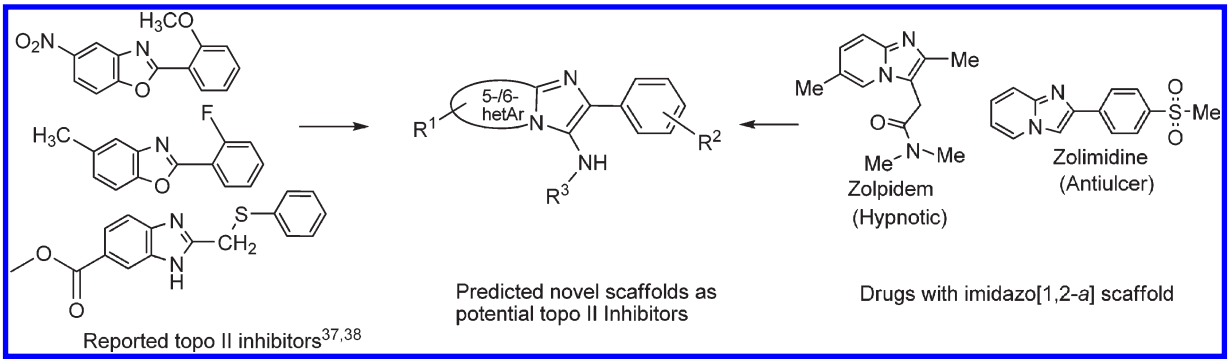

Figure 1. Design of 2-aryl-N-fused imidazoles as potential topo II inhibitors.

now being clinically used, for example, aclarubicin and 4,4-1,2-(ethanediyl)bis(1-isobutoxycarbonyloxymethyl-2,6-piperazinedione) (MST 16)[31] as antineoplastic agents, (*S*)-(+)-1,2 bis(3,5-dioxopiperazinyl)propane (ICRF 187)[32] as cardioprotectors, and suramin and novobiocin as modulators to increase the efficacy of other drugs.[28] In addition, topoisomerase II inhibitors such as etoposide, salvicine, and bis-indolylmethane have been found to possess the ability to regulate the expression of genes involved in invasion,[27] metastasis,[33,34] and angiogenesis.[35]

DNA intercalative or nonintercalative topoisomerase II poisons have been found to possess, in general, some common pharmacophoric features such as planar or semiplanar polycyclic ring (as major groove binder to DNA), a suitable number of hydrogen bond donors and acceptors, and a side chain or ring (as minor groove binder to DNA).[36] However, topoisomerase II catalytic inhibitors regardless of intercalation-ability/non-ability to DNA are structurally unrelated. Various biaryls such as 2-arylbenzimidazole, benzoxazole, and benzthiazole[37,38] are known as topoisomerase II inhibitors. Bicyclic N-fused imidazole, a class of heterocycles represented by marketed drugs, such as zolpidem (hypnotic) and zolimidine (antiulcer), possess structural resemblance to these antitopoisomerase II biaryls (Figure 1).[39,40] As a part of our program aimed at design, synthesis, and bioevaluation of topo-II targeting anticancer agents, we considered that bicyclic N-fused aminoimidazole derivatives could act as potential inhibitors of this enzyme. Recently, we have filed a patent application for the same.[41] The initial molecular docking study of these compounds using FlexX program with ATPase domain of hTopoIIα supported their possible inhibition activity.

In this article, we present the synthesis and biological studies of novel bicyclic N-fused imidazole derivatives. The bioevaluation of these compounds against hTopoIIα was carried out to study decatenation, relaxation, cleavage complex, and DNA intercalation processes. In vitro assays revealed that imidazopyridine, imidazopyrazole, and imidazopyrazine derivatives exhibited potent DNA nonintercalating catalytic inhibition of the enzyme. Being nonintercalating to DNA, these compounds are more specific for binding to the hTopoIIα. Molecular modeling studies and in vitro binding assays revealed that N-fused aminoimidazoles exerted inhibitory effect possibly by blocking the ATP-biding site of hTopoIIα. These derivatives showed potent anticancer activities in kidney and breast cancer cell lines, low toxicity to normal cells, relatively higher potency compared to etoposide and 5-fluorouracil in kidney cancer cell lines, and potent inhibition in cell migration. The compounds were found to exert apoptotic effect in G1/S phase.

Chemistry. Multicomponent reactions (MCRs) offer the elegant performance of multiple reactions into a sequence in one reaction step without isolating the intermediates, atom economy, structural complexity of products (structural economy), bond-forming efficiency (bond-forming economy), convergent synthesis, and the feasibility of introducing maximum chemical diversity elements in one chemical event. They are being increasingly tailored and fine-tuned for synthesizing various heterocyclic scaffolds which are particularly useful in the preparation of diverse libraries of bioactive molecules. As a part of our research program for the preparation of therapeutically relevant heterocyclic compounds, we have recently published several novel and efficient methods for the multicomponent reactions[42] including the Groebke−Blackburn−Bienaymé multicomponent reaction (GBB MCR) of aldehyde, amine and isocyanide toward the syntheses of N-fused imidazoles and their derivatives.[43−45] Keeping in view the potential structural features of N-fused 2-aryl-3-aminoimidazole for exhibiting topoisomerase II inhibition activity, we synthesized a series of investigational compounds with the diverse N-fused imidazole scaffolds with different aryl-substitution at 2-position, moieties linked to amine at 3-position and substitution linked to fused nonimidazole ring (compounds **1**−**31**, Figure 2). They were prepared following our developed GBB MCR methods and the subsequent known transformations (Scheme 1). The bicyclic N-fused alkylaminoimidazo-pyridine, pyrimidine, pyrazine, and pyrazole (compounds **1**−**24**) were synthesized by $ZrCl_4$-catalyzed MCR of corresponding heterocyclic amidine, aldehyde, and isocyanide in PEG-400 at 50 °C (method A) or at 140 °C in case of microwave-mediated dielectric heating process (method B) in good to excellent yields. Tricyclic N-fused imidazobenzimidazole (compound **25**) was prepared by the microwave-promoted dielectric heating process (method B), which was found to be successful compared to the conventional heating method. Free amine-containing N-fused imidazoles (compounds **26**−**30**) were prepared by a domino process of microwave-assisted $ZrCl_4$-catalyzed MCR and subsequent de-*tert*-butylation promoted by HBF_4 (method C). The GBB MCR and subsequent deisooctylation (method D) afforded the preparation of free amine-containing N-fused pyrazole (compound **31**). All the products were identified by ^1H and ^{13}C NMR and IR spectroscopies and confirmed by CHN analysis or HRMS spectroscopy.

BIOLOGICAL STUDIES, RESULTS AND DISCUSSION

Inhibition Studies of Topoisomerase IIα. Several in vitro experiments such as decatenation, relaxation, cleavage complex,

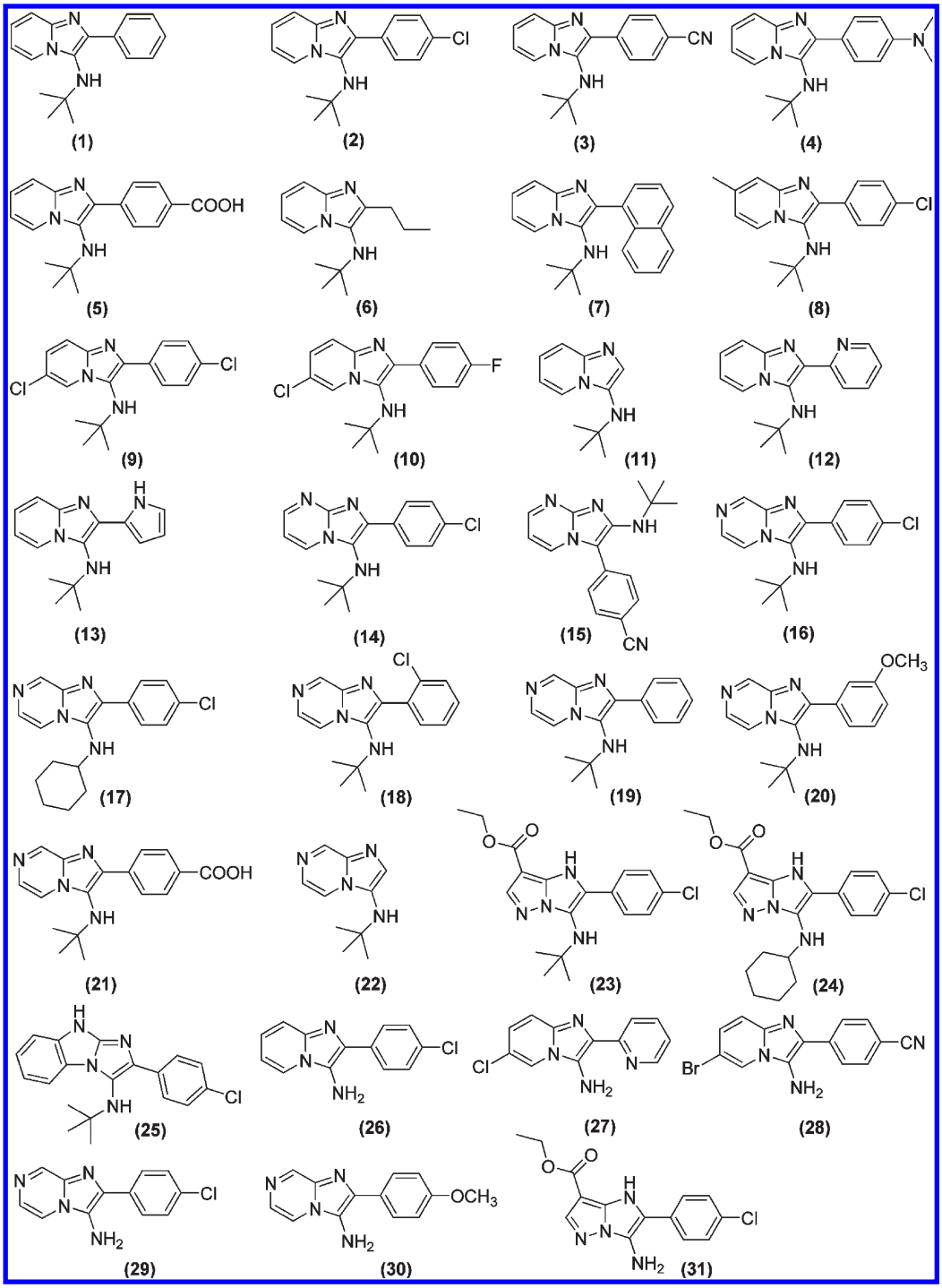

Figure 2. Compounds (**1**−**24**) were synthesized either following method A or method B; compound **25** was prepared following method B; compounds (**26**−**30**) were made by method C and compound **31** by method D.

and DNA intercalation assays and ATPase-kinetics were performed for the bioevaluation of synthesized N-fused imidazole derivatives for their ability to inhibit human DNA topoisomerase IIα (hTopoIIα) and for the investigation of mode of action. A screening kit purchased from TopoGEN, Inc. (Columbus, OH) was utilized. The screening protocols as mentioned in the supplier manual and reported in literature were followed with modification. The concentrations of the reagents were varied according to requirement of our experiments (see Experimental Section).

ATP-dependent decatenation assay, a specific assay for the topoisomerase II inhibition activity, was performed with investigational compounds using kinetoplast DNA (kDNA) as a substrate. Etoposide, a known topoisomerase II-inhibiting anticancer drug, was used as standard. The results are presented in Figure 3A. The decatenation of kDNA by catalytic activity of topoisomerase II forms different decatenation products: nicked (Nck), relaxed (Rel), and supercoiled (SC) DNA. The catenated kDNA appears in agarose gel at the top and cannot enter into the

dx.doi.org/10.1021/jm200235u |*J. Med. Chem.* 2011, 54, 5013–5030

Scheme 1. Methods of Preparation of Investigational Compounds As Potential hTopoIIα Inhibitors

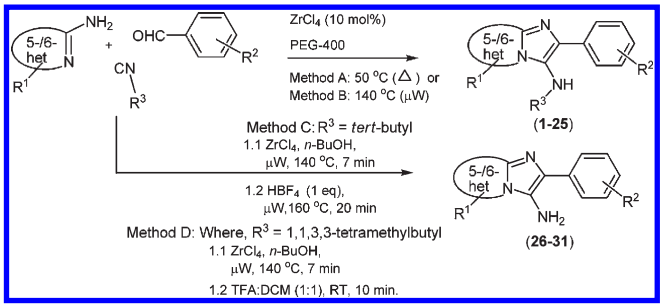

gel because of its overall size while other decatenated products move into. This characteristic pattern was also observed in our experiment. Etoposide showed partial or moderate decatenation because of its known reversible inhibition of topoisomerase IIα.[30] Almost no decatenation activity was observed in the presence of compounds **5**, **9**, **16**, **23**, and **30**. Partial or moderate inhibition of topoisomerase IIα was shown by compounds **12**, **26**, **29**, and **31**, while compounds **2**, **11**, **19**, **21**, and **22** did not show any inhibition. Quantification of decatenation products formed (Nck, Rel, and SC) was done by densitometric data obtained using QuantityOne (BioRad), and the results were compared with etoposide (Figure 3C). In comparison to etoposide, compounds **5**, **9**, **16**, **23**, and **30** were found to show higher inhibition of topoisomerase IIα whereas compounds **12**, **26**, **29**, and **31** exhibited considerable inhibition activity. To confirm their topoisomerase IIα inhibitory potential, relaxation assay using etoposide as positive control was then performed. In this assay, topoisomerase II converts the negatively supercoiled form of substrate pRYG plasmid DNA into relaxed topoisomers that migrate more slowly. Results of our experiment as shown in Figure 3B also reveal the same observation. The products formed (relaxed topoisomers) were quantified, and the results were compared with etoposide (Figure 3D). It was observed that in comparison to etoposide, compounds **5**, **9**, **16**, **23**, and **30** were found to be more potent topoisomerase IIα inhibitors and compounds **12**, **26**, **29**, and **31** exhibited moderate topoisomerase II inhibition. This result of inhibition-potency was found to be consistent with decatenation assay.

Furthermore, to gain insight into the mode of action of investigational potent compounds as topoisomerase II poisons or catalytic inhibitors, cleavage complex assay was performed. Topoisomerase II poisons act by stabilizing enzyme−DNA cleavage complex and thus lead to the formation of linear DNA. In cleavage complex assay, initially the relaxation of the plasmid DNA (pBR322) was allowed to start by addition of topo II and then the compound was added. The gel was run in the presence of ethidium bromide in order to clearly visualize the linear form of the DNA (Figure 4A). In contrast to etoposide (topo II poison), the linear form of the DNA was not visible in the case of investigational compounds (**5**, **16**, **23**, **29**, and **31**). From these results it can be concluded that tested compounds did not act as classical topoisomerase II poisons even at 200 μM concentration. In addition, no linear band was observed when etoposide was preincubated with compound **5**, which revealed its antagonizing effect on topoisomerase II poison. These observations indicate that these N-fused imidazoles act as topoisomerase IIα catalytic inhibitors.

Topo II catalytic inhibitors are of two types: DNA intercalators and nonintercalators.[46] To determine the intercalation/nonintercalation ability of potent compounds, DNA intercalation assay using negatively supercoiled small circular plasmid DNA (isolated from *Escherichia coli*) as substrate was performed.[47] In this assay, 250 ng of plasmid was incubated with ethidium bromide (1 μg/mL), standard drug (etoposide), and investigational compounds. Samples were then loaded in 1% agarose gel, and electrophoresis was run without ethidium bromide. DNA intercalators change the degree of supercoiling or mass of the plasmid DNA, and this change can be detected by observing the retardation in migration during electrophoresis. By performing this assay, it was found that in the presence of intercalative agent (ethidium bromide), there was retardation in the migration of the DNA (Figure 4B), whereas, in the case of etoposide (DNA nonintercalator) and compounds tested, there was no such retardation. This result indicates that the tested compounds are DNA nonintercalators.

From the decatenation, relaxation, stabilization of cleavage complex, and DNA intercalation assays, it is revealed that the investigational compounds (**5**, **16**, **23**, **29**, and **31**) act as DNA nonintercalating hTopoIIα catalytic inhibitors. For the measurement of IC_{50} value, a study of decatenation assay at various concentrations ranging from 10 to 100 μM for the compound **5** (as a representative) was performed. From the plot it was found that compound **5** had IC_{50} value of 52.66 μM (Figure S1, Supporting Information).

Structure−Activity Relationship Study. Upon the basis of the results of topoisomerase II inhibition exhibited by N-fused imidazoles in decatenation and relaxation assays, we synthesized a series of relevant compounds to find out the structure−activity relationship and the pharmacophoric importance of scaffold, moieties/substituents, and their positions (Figure 2). N-Fused imidazoles without aryl-substitution at 2-position (compounds **6**, **11**, and **22**) did not exhibit any inhibition activity of hTopoIIα. The presence of naphthalene moiety at 2-position in imidazopyridine (compound **7**) showed good inhibitory activity, while the presence of *N*,*N*-dimethylphenyl (compound **4**) showed moderate activity. In addition to bicyclic N-fused imidazoles, imidazo-benzimidazole (compound **25**), which is a tricyclic molecule, was also found to be considerably active against topoisomerase II. N-Fused imidazoles containing $-NH_2$ without *tert*-butyl group at 3-position (compounds **26**−**31**), in comparison to their 3-*tert*-butylamine-containing analogues (except compound **30**), showed lower inhibition activity. The compounds **10**, **14**, **18**, **24**, and **28** showed poor activity, and compounds **6**, **8**, **13**, **15**, **17**, **20**, and **27** did not show any inhibition.

All together, suitable combination of nonimidazole scaffold (pyridine, pyrazine, or pyrazole) and its substitution, relevant aryl-substitution at 2-position, and *tert*-butyl-/free-amine at 3-position is crucial for exhibiting inhibitory activity of hTopoIIα.

Molecular Docking Analysis. As potent topoisomerase II inhibitors showed catalytic inhibition of the enzyme and nonintercalation with DNA, we were interested in identifying the potential binding of N-fused imidazole derivatives to the ATPase domain of hTopoIIα in the active site by molecular docking simulation using the FlexX program[48] incorporated in SYBYL 7.1.[49] To validate the molecular docking protocol, ATP and AMPPNP (bound ligand, 5′-adenylyl-β,γ-imidodiphosphate) were initially docked into the crystal structure of ATPase domain of hTopoIIα.[50] The docked AMPPNP found to have similar binding pose as compared to the

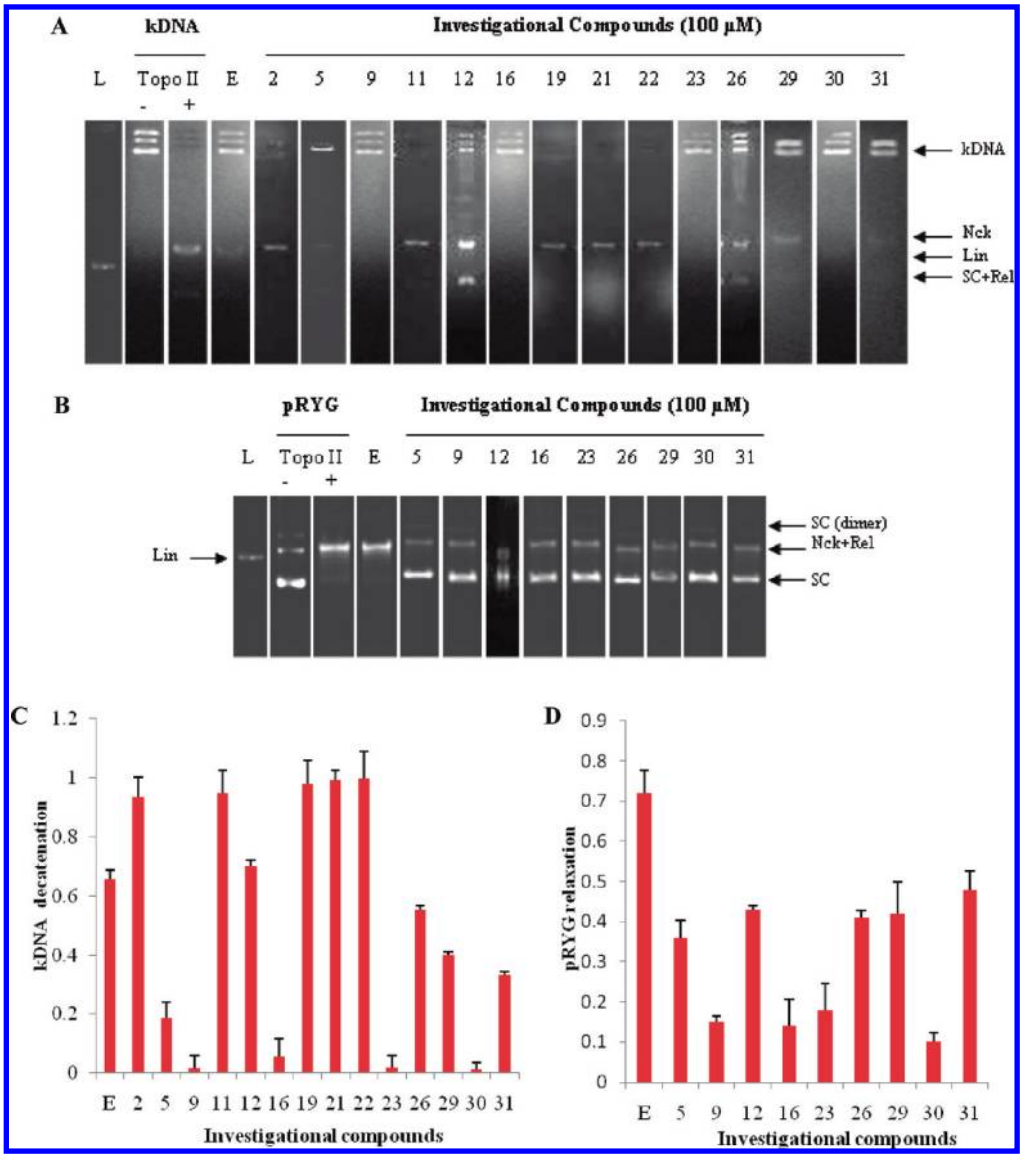

Figure 3. hTopoIIα-inhibitory effect of N-fused imidazoles in decatenation and relaxation agarose gel electrophoresis assays. (A) Decatenation assay: kDNA (intact kinetoplast DNA) was used as substrate, decatenation products formed were Nck (nicked), Rel (relaxed), and SC (supercoiled) DNA. kDNA was treated with hTopoIIα in presence of either 100 μM etoposide or N-fused imidazoles. (B) Relaxation assay: Negatively supercoiled pRYG plasmid DNA was used as substrate and products formed were its relaxed topoisomers. pRYG DNA was treated with hTopoIIα (without ethidium bromide) in the presence of either 100 μM etoposide or investigational compounds. (C) Quantification of product formed in kDNA decatenation assay. (D) Quantification of product formed in pRYG relaxation assay.

cocrystallized ligand with a root mean square deviation (rmsd) of about 1.55 Å. Moreover, superimposition of docked ATP and cocrystallized AMPPNP suggested that ATP also occupies the binding pocket in a similar fashion (Figure 5) and making 3 point contacts with Mg as well as forming key interactions with the residues of ATPase domain similar to that of bound AMPPNP (Figure 6), thus validating the adopted docking methodology. This also suggested that docking protocol is reliable enough to carry out further binding mode analysis of investigational ligands.

In detail, the binding model of ATP with ATPase domain of hTopoIIα (Figure 6) revealed that the amino group of adenine moiety showed hydrogen bonding with the side chain carbonyl oxygen of Asn120 and the two hydroxyl groups of ribose unit formed hydrogen bonding interaction with the side and main chain of Ser149, respectively. Interestingly, the oxygen atoms in the three phosphate group were involved in several interactions with the ATPase domain, viz: hydrogen bonding with the main chain nitrogen atom of the residues Arg162, Asn163, Gly164, Tyr165, Gly166, and Ala167 (Walker A consensus motif). In addition, these phosphate groups also showed hydrogen bonding interactions with the side chains of residues Asn91, Ser148, Asn150, Lys168, and Gln376. Consistent with the interactions shown by the bound ligand AMPPNP with the crystal structure of ATPase domain, the docking model of ATP also showed that phosphate group forms a salt bridge with the highly conserved Lys378 from the QTK-loop (Gln376-Thr377-Lys378) of the transducer domain.

The highly conserved Walker A consensus ATP binding site of hTopoIIα is composed of residues 161−166 (GXXGXG)[51] and is important for the binding of ATP as well as for the catalytic inhibitors acting on ATPase domain. Wessel et al. performed site-

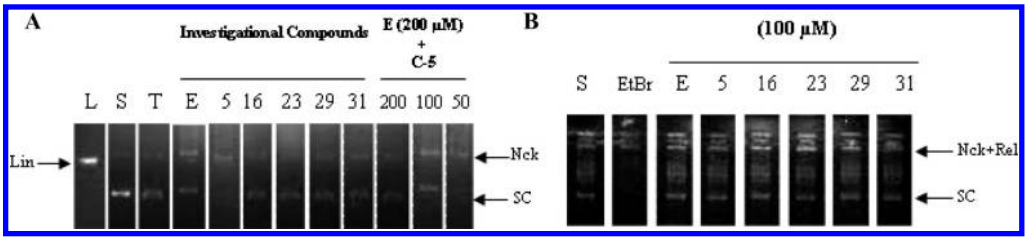

Figure 4. (A) Stabilization of cleavage complex assay: After treatment with hTopoIIα, negatively supercoiled plasmid was incubated with either 100 μM etoposide or investigational compounds or both (for testing antagonizing effect, last 3 lanes). The agarose gel was run in excess of ethidium bromide to check the formation of linear (Lin) band. In contrast to etoposide, a linear band was not observed in any of the tested compounds. Compound **5** was found to antagonize the effect of etoposide as topoisomerase II poison. (B) DNA intercalation assay: Negatively supercoiled plasmid was incubated with 1 μg/mL ethidium bromide or 100 μM etoposide or investigational compounds. Agarose gel electrophoresis (without ethidium bromide) was run, which clearly showed retardation in the migration of ethidium bromide (intercalator)-treated DNA, whereas no retardation was observed in DNA treated with investigational compounds.

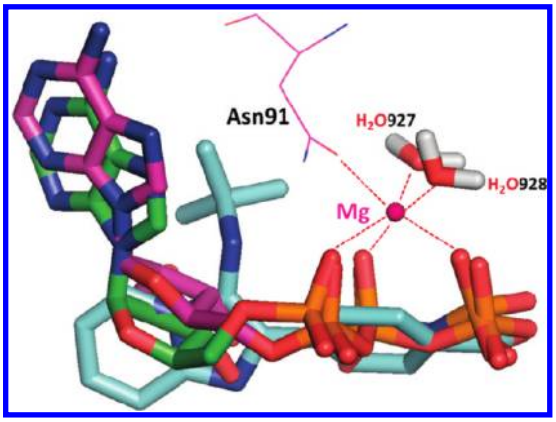

Figure 5. Superimposition of cocrystallized AMPPNP (magenta), best docked pose of ATP (green) and compound **5** (cyan) in the hTopoIIα ATP binding site. The magenta sphere represents Mg cation showing octahedral coordination geometry.

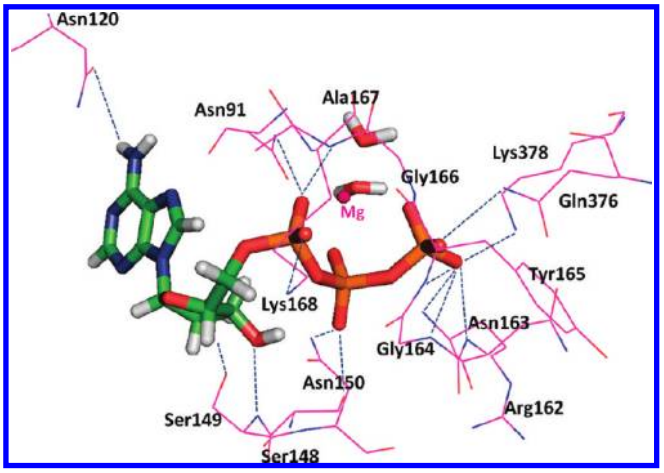

Figure 6. Binding model of ATP as revealed from FlexX docking in hTopoIIα ATP binding site. The blue dashed lines represent hydrogen bonds and magenta sphere represents Mg cation. H-bond distances (in Å) between heteroatoms of ligand and amino acid residues are as follows: Asn91 (2.71), Asn120 (3.37), Ser148 (2.53), Ser149 (2.87), Asn150 (3.12), Arg162 (3.12), Asn163 (2.78), Gly164 (3.01), Tyr165 (2.59), Gly166 (2.59), Ala167 (2.98), Lys168 (2.72), Gln376 (2.93), and Lys378 (2.95).

directed mutagenesis studies and found that the Arg162Gln and Tyr165Ser mutations (in the ATP binding site) lead to drug resistance.[52,53] Moreover, the importance of residue Gly164 was established by Skouboe et al.[54] The results of their study revealed that ATP binding was inhibited by mutation of residue Gly164 to Ile. The docking model of ATP as discussed above also showed that the residues in Walker A motif are crucial for the binding of ATP, thus suggesting the reliability of docking methodology.

Further studies demonstrated that N-fused imidazoles might bind at the ATP site of hTopoIIα ATPase domain. The superimposition of the cocrystallized AMPPNP, docked ATP, and most active compound **5**, which is also a best scored (−35.45) compound according to the docking results (Table 1), indicate that the benzene ring and *para* carboxylic group overlap with the phosphate groups of AMPPNP and ATP in the ATP binding site (Figure 5). This observation implies that the substitution at 2-position of N-fused imidazole ring is essential for the competitive binding with ATP. This is also consistent with the experimental results and SAR study because the compounds **6** and **11** lacking substitution at 2-position of N-fused imidazole ring were found to be inactive as catalytic inhibitors.

Table 1 demonstrates the result of the molecular docking along with hydrogen bonding and metal ion interactions of compounds **5**, **23**, **30**, and **31** (potent topoisomerase II inhibitors), compounds **26** and **29** (moderately active), and compounds **6** and **11** (inactive). As indicated in the interaction model between most active compound **5** and ATPase domain (Figure 7), the carboxylic group at *para* position of benzene ring formed multiple hydrogen bonding interactions with the backbone nitrogen atom of the residues Arg162, Asn163, Gly164, Tyr165, and Gly166. The same carboxylic acid group also formed hydrogen bonding interactions with the side chain of residues Gln376 and Lys378. In addition, imidazole nitrogen of compound **5** showed hydrogen bond with the side chain of Ser148 and backbone nitrogen atom of Ser149, respectively. Most notably, the benzene ring substituted at 2-position in compound **5** showed an effective π interaction with the magnesium cation (magenta sphere in Figure 7), and the 3-substituted *tert*-butyl group of compound **5** was involved in the hydrophobic interaction with the Asn91, Arg98, and Asp94. Moreover, the same *tert*-butyl group may also be involved in weak CH···O type of interaction with the side chain of residues Asn91 and Asp94, which may give extra stability to the enzyme−ligand interactions. Additionally, pyridine ring fused with imidazole also showed hydrophobic interaction with residues Ile141 and Phe142. The docking results for other active compounds (**23**, **30**, and **31**) also predicted favorable

Table 1. FlexX Docking Results for Some of the Synthesized Compounds and Substrate ATP in Presence of Two Conserved Water Molecules in hTopoIIα ATP Binding Site

			hydrogen bonding interactions		
compd	experimental activity	FlexX score	backbone	side chain	interaction with Mg cation
ATP (−4)[a]	substrate	−84.06	Ser149, Arg162, Asn163, Gly164, Tyr165, Gly166, Ala167	Asn91, Asn120, Ser148, Ser149, Asn150, Lys168, Gln376, Lys378	ionic interaction
5 (−1)[a]	good	−35.45	Ser149, Arg162, Asn163, Gly164, Tyr 165, Gly166	Gln376, Lys378	π interaction
31	good	−23.53	Ser149, Gly164, Ala167	Asn91, Ser148, Ser149, Asn150 (4)	ionic interaction
23	good	−22.73	Arg162, Asn163, Gly164	Asn91, Ser148 (2), Ser149, Asn150	ionic interaction
30	good	−20.20	Asn91	Asp94, Ser148, Asn150 (2)	π interaction
29	moderate	−11.50	Asn91	Asn150	π interaction
26	moderate	−10.86	Asn91		π interaction
11	not active	−10.23		Asn150, Ser148	no interaction
6	not active	−8.78	Ser149	Asn95, Ser149	no interaction

[a] Values in bracket indicates the total charge on the compound, while other compounds are considered as neutral.

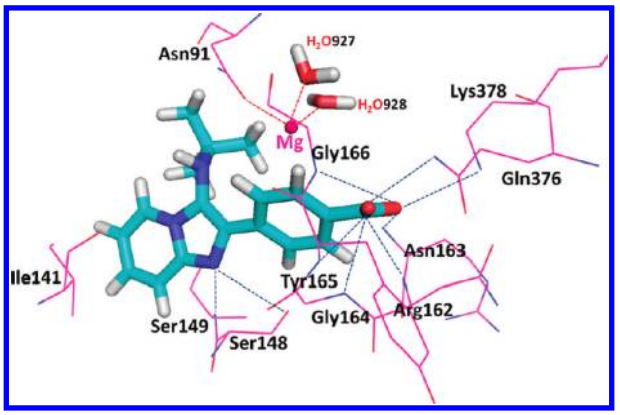

Figure 7. Binding model of active compound **5** (cyan) as revealed from FlexX docking in hTopoIIα ATP binding site. The blue dashed lines represent hydrogen bonds and magenta sphere represents Mg cation. H-bond distances (in Å) between heteroatoms of ligand and amino acid residues are as follows: Ser148 (3.33), Ser149 (2.56), Arg162 (2.83), Asn163 (2.25), Gly164 (3.03), Tyr165 (2.99), Gly166 (3.09), Gln376 (2.98), and Lys378 (3.43).

Table 2. Averaged Binding Free Energy Results for Enzyme−Ligand (Compound 5) Complex along with Its Different Energy Components

terms[a]	energy (kcal/mol)	terms[a]	energy (kcal/mol)	terms[a]	energy (kcal/mol)
ΔE_{ELE}	−253.50	ΔPB_{SUR}	−5.54	ΔGB_{SUR}	−5.54
ΔE_{VDW}	−36.21	ΔPB_{CAL}	231.52	ΔGB	227.00
ΔE_{GAS}	−289.71	ΔPB_{SOL}	225.99	ΔGB_{SOL}	221.46
		ΔPB_{ELE}	−21.98	ΔGB_{ELE}	−26.50
		ΔPB_{TOT}	**−63.72**	**ΔGB_{TOT}**	**−68.25**

[a] The meaning of the different terms in this table is as follows: ELE = electrostatic energy as calculated by the MM force field; VDW = van der Waals contribution from MM; INT = internal energy arising from bond, angle and dihedral terms in the MM force field (this term always amounts to zero in the single trajectory approach); GAS = total gas phase energy (sum of ELE, VDW and INT); PBSUR/GBSUR = nonpolar contribution to the solvation free energy calculated by an empirical model; PBCAL/GB = the electrostatic contribution to the solvation free energy calculated by PB or GB respectively; PBSOL/GBSOL = sum of nonpolar and polar contributions to solvation; PBELE/GBELE = sum of the electrostatic solvation free energy and MM electrostatic energy; PBTOT/GBTOT = final estimated binding free energy calculated from the terms above (kcal/mol).

interactions between the compounds and key residues at the ATPase domain, similar to that observed in the interaction model of compound **5** (Table 1).

From the detailed analysis of active compounds binding model, it was found that all potent and moderately active compounds showed an effective interaction with the magnesium, either via π interaction (**5**, **26**, **29**, and **30**) or ionic interaction (**23** and **31**) (Table 1). This type of interaction was missing in case of the inactive compounds (**6** and **11**), as they lack benzene ring at 2-position of N-fused imidazole system. These observations are consistent with the results for the docking of pyranonaphthoquinones into the ATP binding pocket of hTopoIIα, reported by Jimenez-Alonso et al.[30] Moreover, the inactive compounds (**6** and **11**) showed less favorable docking score and missed the key interactions shown by the active compounds and ATP with the residues of ATPase domain. The binding model of the active compounds (**5**, **23**, **30**, and **31**) also revealed that they share common hydrogen bonding interactions with the key residues of the ATPase domain as shown by ATP (Table 1). Therefore, these compounds can effectively compete with the ATP for occupying the ATP-binding pocket of hTopoIIα.

Thus, molecular modeling studies performed on a small number of N-fused imidazole derivatives from our chemical archives suggest that some compounds are catalytic inhibitors acting via occupying the ATP binding pocket of ATPase domain of hTopoIIα and making favorable interactions with its key residues.

Molecular Dynamics Simulation Analyses. The molecular docking analyses of compound **5** in the active site of ATPase domain of hTopoIIα provided a pose which explains most of the enzyme−ligand (inhibitor) interactions. To validate that these interactions are realistic, stability of the

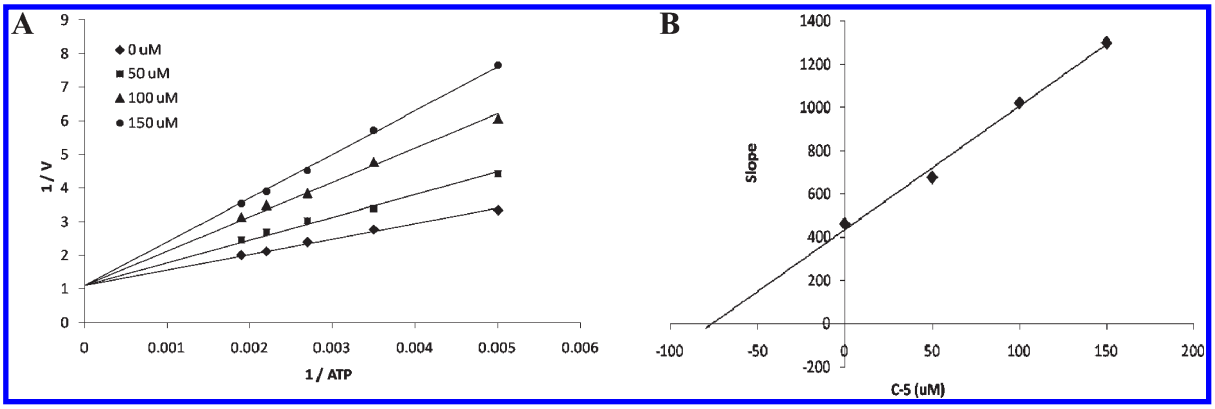

Figure 8. Concentration-dependent inhibition of topoisomerase IIα−ATPase activity by compound **5**. (A) Lineweaver−Burk plot of the ATPase activity assay. (B) Slopes of the respective lines against different concentrations of compound **5**.

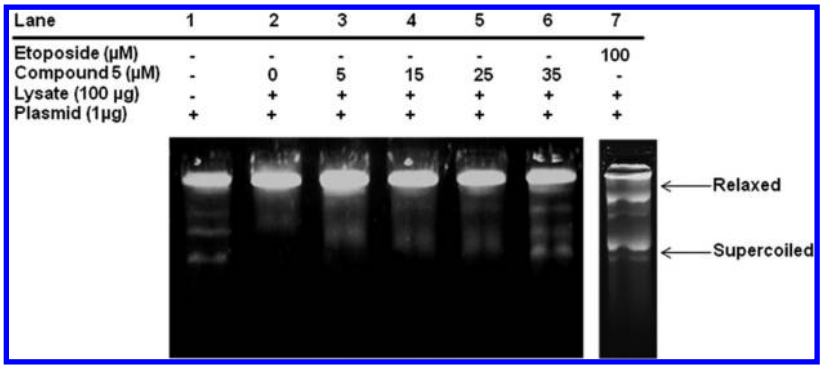

Figure 9. Inhibition of topoisomerase activity by compound **5** in HEK 293 cells. Reaction was carried out according to the protocol described in Experimental Section. Image shown here is representative of three independent experiments.

enzyme−ligand complex was assessed by MD simulations implementing AMBER 10 software.[55]

The energy vs time plot showed an unperturbed energy profile during the production run, confirming the stability of complex (Figure S3, Supporting Information). The estimated fluctuation in the rmsd of the enzyme−ligand complex during the equilibration to production run is less than 1 Å, again confirming the stability of complex (Figure S4, Supporting Information). The hydrogen bond analyses confirmed the persistence of hydrogen bonding interactions of ligand (compound **5**) with residues Arg162, Asn163, and Lys378, while hydrogen bonding with residues Ser149, Gly164, and Gln376 are less consistent (Figure S5a,b, Supporting Information).

The prediction of binding affinity of ligands was performed on the basis of binding free energy calculations using molecular mechanics Poisson−Boltzmann surface area (MM-PBSA) and molecular mechanics generalized Born surface area (MM-GBSA) protocol.[56,57] In the present study, we estimated the different components of interaction energy that contribute to binding, these include van der Waals, electrostatic, polar solvation, and nonpolar solvation interaction energies. Table 2 shows the averaged binding free energy results for enzyme−ligand complex along with their different energy components (see Supporting Information for more detail). The binding free energy calculated by the above two methodologies, $\Delta G_{MM/PBSA}$ and $\Delta G_{MM/GBSA}$ for enzyme−ligand (compound **5**) complex are −63.72 and

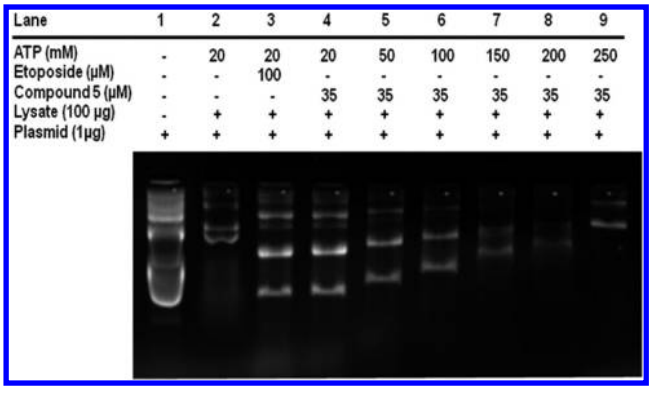

Figure 10. ATP reverts the topoisomerase inhibition of compound **5**. The image shown here is representative of three independent experiments.

−68.25 kcal/mol, respectively. ΔPB_{TOT} accounts of total relative binding free energy which equal to $\Delta E_{GAS} + \Delta PB_{SOL}$ which shows that most of the contribution to the binding free energy comes from the electrostatic component, whereas van der Waals contribution is comparatively less. This is due to the fact that ligand (compound **5**) has negatively charged carboxylic group at *para* position of benzene, which is forming favorable hydrogen bonding and electrostatic interactions with the backbone nitrogen atom of Walker A consensus motif residues.

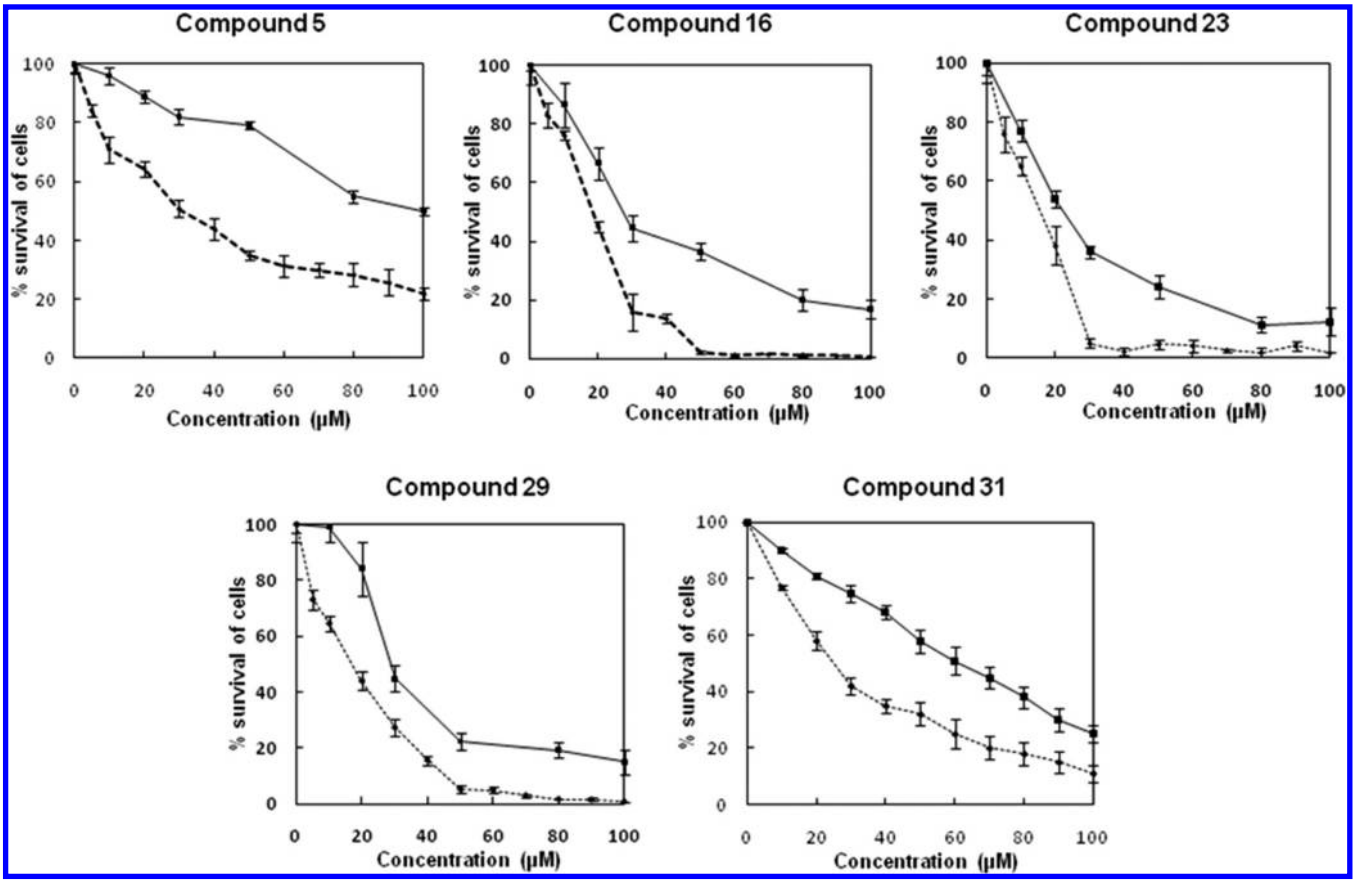

Figure 11. Clonogenic cell survival after treatment with indicated compounds of various concentrations for 48 h. Dotted lines represent the % survival of HEK-293 cells, and bold lines represent % survival of Vero cells, respectively. Data represented here are mean of three independent experiments, and values are mean ± SD.

ATPase Assay. Molecular docking studies of N-fused aminoimidazole (compound **5**) as mentioned above suggested their catalytic mode of inhibition, plausibly via blocking the ATP-binding site of topoisomerase. To prove this observation, an in vitro ATPase assay for DNA dependent ATP hydrolysis of hTopoIIα was performed using compound **5**. Different concentrations of ATP (200, 280, 360, 440, and 520 μM) and 6 units of topoisomerase II were incubated with compound **5** of a fixed concentration 0, 50, 100, and 150 μM, respectively. Lineweaver–Burk plot of the ATPase assay (Figure 8A) shows decrease in K_m while no change in V_{max}. This indicates that compound **5** is a competitive inhibitor of ATP.[58,59] Calculated K_i value for compound **5** was 75 μM (Figure 8B).

Inhibition of Topoisomerase Activity in HEK 293 Cells. A DNA unwinding assay was performed using compound **5**, HEK 293 nuclear lysate, and plasmid DNA following the procedure as described in the Experimental Section. For nuclear cell lysate without compound **5**, supercoiled plasmid was relaxed or linear and thus did not enter into the 0.9% agrarose gel (Figure 9). This may be because of topoisomerase activity in nuclear lysate of HEK 293 cells. However, in the presence of compound **5** with increasing concentrations, the supercolied DNA topoisomer was found to be more and at 35 μM concentration good inhibition (compare lane 1 with 6) of topoisomerase activity was found (Figure 9).

ATP Dependent Plasmid Relaxation Assay. In addition to in vitro ATPase kinetic studies, an ATP dependent plasmid relaxation assay of topoisomerase activity was performed using HEK 293 nuclear lysate, compound **5**, and ATP of various concentrations. Figure 10 illustrates that in the absence of compound **5**, topoisomerase effectively relaxes the supercoiled form of the plasmid (lane 2), but in the presence of compound **5** and etoposide (positive control), topoisomerase activity was inhibited and a more supercoiled form of the plasmid was observed (lane 3 and 4, respectively). Interestingly, when a fixed concentration of compound **5** and increasing doses of ATP were added to the reaction mixture, increasing amount of the relaxed form of the plasmid was observed. Thus, it appears that ATP with higher concentrations displaces compound **5** from the active site of topoisomerase (lane 5 to 9). This implies that ATP and compound **5** are competitive inhibitors of topoisomerase ATP binding domain which is in accordance with in vitro hTopoIIα-ATPase study.

Anticancer Activities of Compounds 5, 16, 23, 29, and 31. *Clonogenic Cell Survival Assay of Kidney Cancer Cells (HEK 293).* The clonogenic cell survival assay is a long-term cell viability assay that determines the ability of a single cell to proliferate indefinitely, thereby retaining its reproductive ability to form a colony or a clone. This assay was done to investigate the anticolony-forming potential of N-fused imidazoles **5**, **16**, **23**, **29**, and **31** in kidney cancer cell lines (HEK 293) as compared to normal kidney epithelial cells (Vero). Each compound showed colony formation inhibition in a concentration-dependent

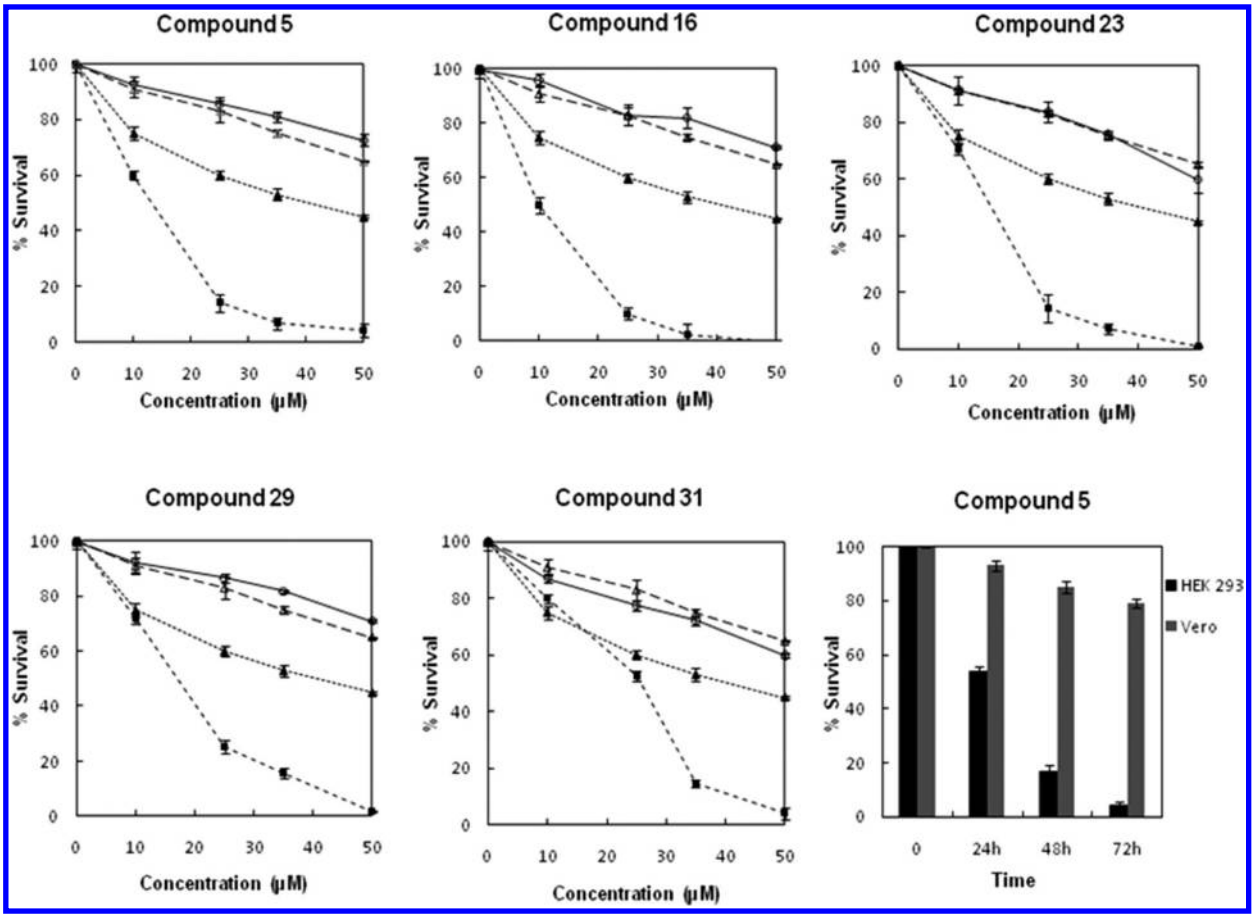

Figure 12. MTT cell survival assay. Cells were treated with investigational compounds and etoposide of various concentrations for 48 h and the assay was carried out according to the protocol as described in Experimental Section. The sign —○—, ---△---, · · ·▲· · ·, and ---■--- represent for Vero cells/investigational compound, Vero/etoposide, HEK 293/etoposide, and HEK 293/investigational compound, respectively. Bar diagram represents the effect of compound **5** (12 μM) on Vero and HEK 293 cell survival with time. Data represented here are the mean of three independent experiments and values are mean ± SD.

manner (Figure 11). HEK 293 cells were more susceptible than Vero cells to the tested compounds.

LC_{50} (the concentration required to kill half the cells in the cell culture) exhibited by compounds **5**, **16**, **23**, **29**, and **31** were 30, 20, 15, 16, and 25 μM, respectively, in HEK 293 cells and 98, 25, 22, 28, and 62 μM, respectively, in Vero cells (Figure 11). From these data it appears that all the tested compounds offered more anticolony-forming ability in kidney cancer cells compared to normal kidney epithelial cells.

MTT Cell Survival Assay of Kidney Cancer Cells (HEK 293). To investigate cytotoxicity of compounds (**5**, **16**, **23**, **29**, and **31**) in both HEK 293 and Vero cells, an MTT assay was carried out.[60] Cell survival was measured after treatment of cells with the investigational compounds for 48 h. With increasing concentration of the compounds, the cell viability of HEK 293 significantly decreased in comparison to Vero cells. Compound **5**, **16**, **23**, **29**, and **31** killed 50% HEK 293 cells (LC_{50}) at 12, 10, 15, 17, and 25 μM, respectively. However, any compound of even 100 μM concentration did not cause 50% cell death in Vero cells (Figure 12). Etoposide showed LC_{50} at 90 μM in HEK 293 cells while it exerted similar effect in Vero cells. To investigate relative survival of cells with time, a separate set of experiments was performed by treating the cells with compound **5** of a fixed concentration (12 μM) for different time intervals. It was noticed that more than 50% HEK 293 cells died after 48 h exposure of compound without considerably affecting the Vero cells (Figure 12, bar diagram).

*Cell Survival Activity of Compound **5** and 5-Fluorouracil in Cancer Cell Lines.* To check the relative potency of anticancer activities of investigational N-fused imidazoles with a clinically used anticancer drug 5-fluorouracil,[61] an experiment using kidney cancer cell line was performed (Figure 13A). Cells were treated separately with different compounds and 5-fluorouracil of various concentrations for 48 h, and then cell survival was measured by MTT assay. All the compounds showed a characteristic cell survival profile. LC_{50} for compound **5**, **16**, **23**, **29**, and **31** were found to be 14, 10, 15, 17, and 27 μM, respectively. However, 5-fluorouracil caused 50% cell death at 30 μM concentration.

To investigate further the cytotoxic effect of compound **5** on another cell line such as breast cancer, a MTT assay was performed using breast cancer (MCF 7) cells and normal breast epithelial cells (MCF 10A). Figure 13B illustrates the anticell survival potential of compound **5** on MCF 7 and MCF 10A cells. Compound **5** caused 50% cell death at 15 μM in

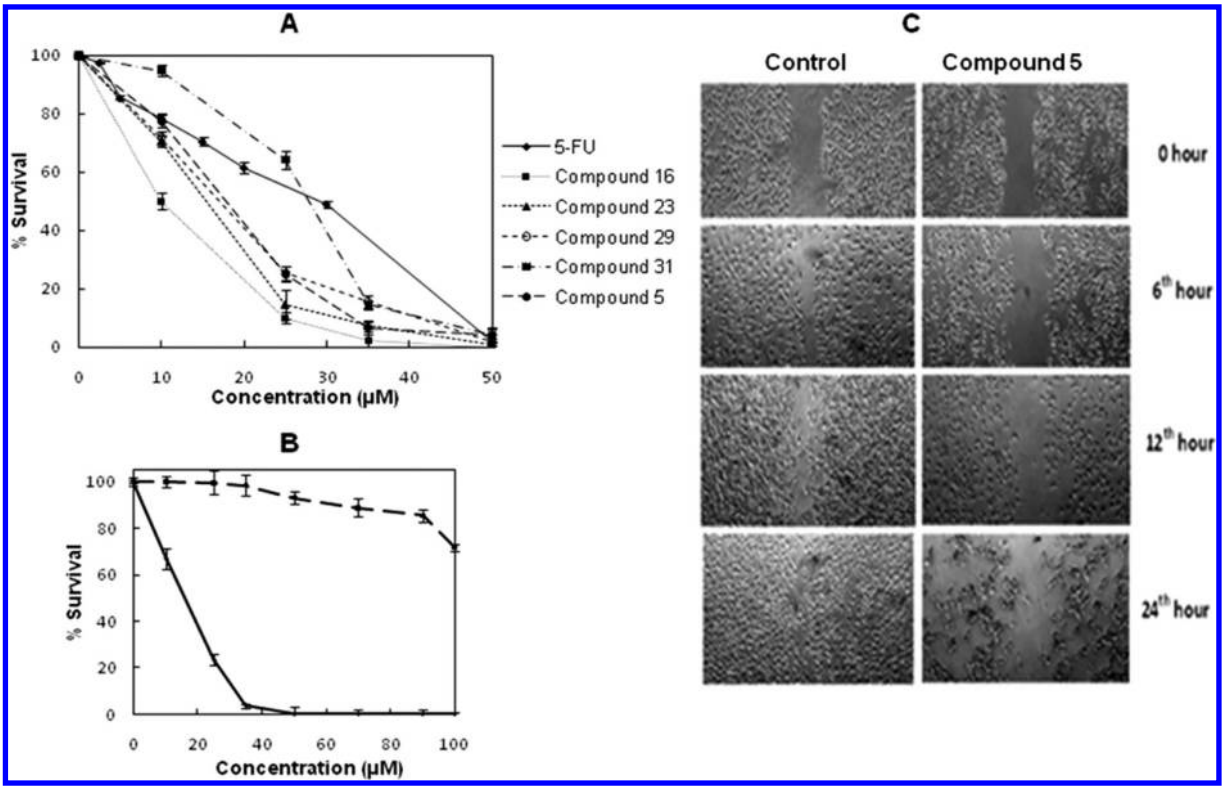

Figure 13. Effect of compound **5** on cell survival and migration in anchorage dependent manner. (A) Comparison of anticell survival activity of compounds (**5**, **16**, **23**, **29**, and **31**) with 5-fluorouracil in HEK 293 cells by cell survival assay. (B) Graphical presentation for the effect of compound **5** on breast cancer cells (MCF 7) as compared to normal breast epithelial cells (MCF 10A). Data represented here are the mean of three independent experiments and values are mean ± SD. (C) Effect of compound **5** on cell migration in HEK 293 cells. After making the wound with a sterile micro tip, the cells were cultured in absence and presence of compound **5** (25 μM). Results shown here are the best of three independent experiments.

MCF 7 cells, whereas 75% cell survival was noted at 100 μM in MCF 10A ($p < 0.05$) (Figure 13B).

*Anti-Cell Migratory Activity of Compound **5** in HEK 293 Cells.* To examine the inhibitory effect of compound **5** on anchorage-dependent cell migration, a wound healing assay was performed according to protocol described in Experimental Section. The gap of the treated cells increased with time in contrast to the untreated cells (Figure 13C). In untreated cells, the gap was completely filled at 24 h. Thus, this assay in conjunction with the assays as discussed above (clonogenic and MTT cell survival) reveals that compound **5** possesses the inhibitory activities of colony formation, viability, and migration of cancer cells (Figure 11−13).

*Apoptosis by Compound **5** in HEK 293 Cells.* Apoptosis of HEK 293 cells were determined after 48 h of treatment with compound **5** using 4′-6-diamidino-2-phenylindole (DAPI) nuclear staining method (Figure 14A). It was observed that apoptotic nuclei increased with increasing concentrations of compound **5** (Figure 14B). It was noticed that at 15, 25, and 35 μM concentrations, compound **5** caused approximately 20, 40, and 80% apoptosis, respectively. To further confirm the apoptotic effect of this compound in HEK 293 cells, a study of protein levels of some apoptotic markers such as Caspase-3, Bax, Bcl-XL, and PARP cleavage was performed by Western blot analysis (Figure 14C). The expression of Bcl-XL was reduced when cells were exposed to compound **5** of increasing concentrations (0, 15, and 25 μM). In contrast to Bcl-XL, the expression of Bax and Caspase-3 was increased. The level of cleaved PARP product (86 KD) was higher in the treated cells than untreated cells and increased with increasing concentrations of the drug. As expected, the expression of β-actin, which served as a loading control, remained unaltered. These relative expressions of relevant apoptotic markers including the increasing Bax/Bcl-XL ratio, Caspase-3, and PARP cleavage clearly indicate that compound **5** causes apoptosis in cancer cells.

*Regulation of Cell Cycle by Compound **5** in Kidney Cancer Cells.* To check the regulation of cell cycle profile and to understand the mechanism by which compound **5** can induce apoptosis, we analyzed the kidney cancer cells after treatment with compound using fluorescence activated cell sorter (FACS) by staining with propidium iodide. Figure 14D demonstrates the cell cycle profile of HEK 293 cells after exposure to compound **5** for 48 h. A sharp dose-dependent increase in apoptosis (Sub G_0) was observed with the drug. At 15, 25, and 35 μM concentrations, the percentage of apoptotic nuclei were noted to be 24.61 ± 1.5, 27.46 ± 1.5, and 49.29 ± 1.0, respectively ($p < 0.05$). It was observed that the percentage of G1-DNA population was significantly decreased with increasing concentrations of compounds **5** (approximately 21.52% at 35 μM in contrast to 61.7% in untreated cells). It was also noticed that S phase DNA population decreased (less than 10%) in comparison to untreated cells. However, no significant change was noted in G2/M phase. A histographical presentation of cell cycle profile of HEK 293 after treatment with compound **5** is provided (Figure 14E). Thus, from the above

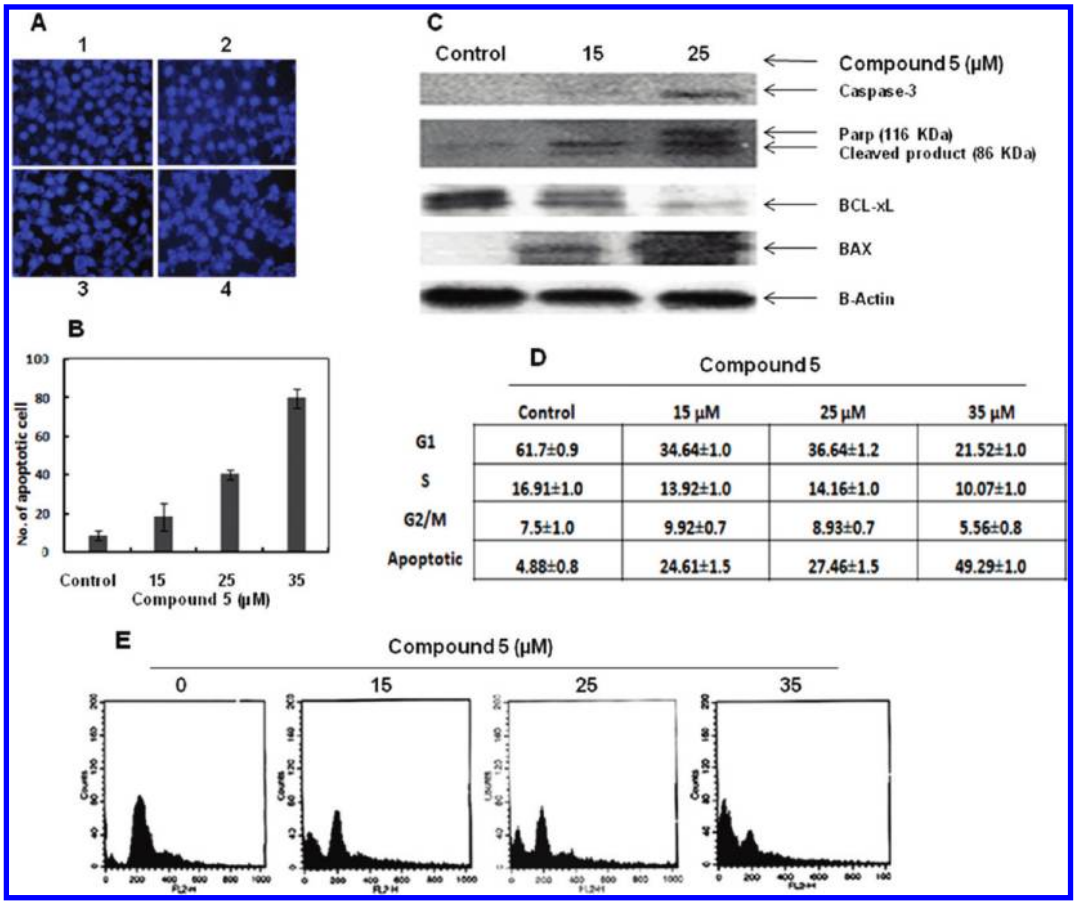

Figure 14. Regulation of cell cycle profile and apoptosis caused by compound **5** in HEK 293 cells. Cells were treated for 48 h with different concentrations of compound **5**, and then experiments were carried out according to the method as described in Experimental Section. (A) DAPI nuclear staining. Images are one of the three replicates of the individual experiments. Images 1, 2, 3, and 4 represent cells treated with compound **5** of 0, 15, 25, and 35 μM, respectively. (B) A graphical presentation of apoptotic nuclei of (A) ($P < 0.05$). (C) Western blot analysis of whole cell extracts. Lower panel (β-actin) represent equal loading of each lane. (D) Tabular form of percentage of DNA in each phase of cell cycle, and (E) graphical presentations of FACS analysis of (D). Here the data presented are the best of three independent experiments.

results it appears that cancer cells undergo significant apoptosis in G1/S boundary phase of cell cycle.

CONCLUSIONS

In conclusion, several derivatives of bicyclic N-fused aminoimidazoles were synthesized by multicomponent reaction and its tandem process of dealkylation. The hTopoIIα-inhibitory activity of these new chemical entities (NCEs) was tested in decatenation, relaxation, and cleavage complex in vitro assays. DNA intercalation assay was performed with EtBr as positive control. It revealed that five compounds, **5**, **16**, **23**, **29**, and **31**, acted as potent DNA nonintercalating topoisomerase IIα catalytic inhibitors. Being nonintercalating to DNA, these compounds are more specific for binding to the hTopoIIα. Molecular docking studies using FlexX program incorporated in SYBYL 7.1 of potent N-fused aminoimidazoles into the ATPase domain of hTopoIIα, and the molecular dynamics simulation studies suggested their catalytic mode of inhibition, plausibly via blocking the ATP-binding site of enzyme. This ATP-competitive inhibition by N-fused imidazole was also further evident by ATPase kinetic study and ATP dependent plasmid relaxation assay of nuclear lysate using compound **5**. Clonogenic and MTT cell survival assay of kidney cancer cells (HEK 293) revealed that these derivatives showed potent anticancer activity and low toxicity to normal cells. Compared to etoposide and 5-fluorouracil, these compounds were found to be more potent in anticancer activity (kidney cancer cells). Compound **5**, chosen as a representative, was found to be potent anticancer agent in breast cancer cells (MCF 7) while relatively less toxic to normal cells (MCF 10A). It showed also the anticell migration. DAPI nuclear staining and the study of expression level of apoptotic marker proteins revealed that compound **5** caused programmed cell death, and the FACS analysis indicated that the apoptosis occurred in G1-S boundary phase of cell cycle. The specific topoisomerase IIα catalytic inhibition activity via ATPase domain-binding, inhibition of topoisomerase in cancer cells, apoptotic affect in G1/S boundary phase, known increased expression of topoisomerase IIα enzyme in G1/S phase, and the molecular docking studies of potent N-fused aminoimidazoles indicate that these novel compounds exerted the anticancer activity by programmed cell death via catalytic ATPase domain-inhibition of topoisomerase IIα. These results will aid in the rational design of novel agents that target the catalytic inhibition of hTopoIIα and will provide insights into the discovery of novel anticancer agents.

EXPERIMENTAL SECTION

Chemistry. The compounds **1**−**24** were prepared following the reported method A or B as mentioned in Scheme 1.[43,44] Compound **25**

was synthesized following the reported method B. The method C afforded the preparation of compounds **26**−**30**.[45] Compound **31** was synthesized by reported method D. All the products were identified by ^{1}H and ^{13}C NMR and IR spectroscopies and confirmed by elemental analysis or HRMS spectrometry. Analytical HPLC was used to determine the purity of the compounds and the purity was found to be greater than 95%. All these data are provided in Supporting Information.

Biological Assay. The testing of new chemical entities was performed using a commercially available topoisomerase II drug screening kit, purified hTopoIIα, and etoposide purchased from TopoGEN, Inc. (Columbus, OH). A stock solution of etoposide of concentration, 10 μM in DMSO, was prepared and stored at −20 °C. Synthesized compounds were also stored at −20 °C. The assay protocols followed were same as mentioned in the supplier manual, except the concentration of the reagents which were varied according to the requirement.

TopoII-Mediated DNA Decatenation Assay. In agarose gel decatenation assay, kinetoplast DNA (kDNA) was used as a substrate. All the reactions were assembled on ice in micro centrifuge tubes. Briefly, 2−4 units of purified human topoisomerase II, 150 ng of catenated kDNA, and 100 μM drug dissolved in DMSO were combined in freshly prepared 5× complete reaction buffer. The reaction mixture was brought to a final volume of 20 μL with deionized, distilled H_2O. For the standard assay method, the order of addition to the assay was H_2O, 5× assay buffer (buffer A: 0.5 M Tris-HCl (pH 8), 1.50 M sodium chloride, 100 mM magnesium chloride, 5 mM dithiothreitol, 300 μg of bovine serum albumin/mL; buffer B: 20 mM ATP in water), kDNA, followed by either test compound or standard drug and finally topoisomerase II. The incubation was run at 37 °C for 30 min. The reaction was then stopped with 10% SDS, followed by digestion with proteinase K and further incubated at 37 °C for 15 min. Topological forms of kDNA were resolved by running 1% agarose gel electrophoresis in Tris-acetate-EDTA (TAE) buffer containing 0.5 μg/mL ethidium bromide and further destained with water for 20 min. The bands of kDNA and decatenated products were visualized by UV trans-illumination, and the products were quantified with QuantityOne (BioRad).

TopoII-Mediated DNA Relaxation Assay. In relaxation assay supercoiled plasmid DNA (pRYG) was used as substrate. Reaction mixture contained freshly prepared 5× complete buffer (A: 0.5 M Tris-HCl (pH 8), 1.50 M sodium chloride, 100 mM magnesium chloride, 5 mM dithiothreitol, 300 μg of bovine serum albumin/mL; buffer B: 20 mM ATP in water), 250 ng of supercoiled plasmid DNA (pRYG), followed by either test compound or standard drug (100 μM) and finally topoisomerase II (2−4 units) in a total of 20 μL. Relaxation was employed at 37 °C for 30 min and stopped with 10% SDS followed by digestion with proteinase K and further incubated at 37 °C for 15 min. Electrophoresis was carried out in a 1% agarose gel in TAE buffer without ethidium bromide. Further the gel was stained with ethidium bromide (0.5 μg/mL) for 15 min and destained with water for 20 min and photographed using BioRad. Quantification of the products was carried out as mentioned in decatenation assay.

Stabilization of the Cleavage Complex. Cleavage complex assay was performed using supercoiled plasmid DNA (pBR322) following the protocol of the relaxation assay as discussed above with modification that 8 units of hTopoIIα was added 3−5 min before the addition of the compound. Reaction mixture was incubated at 37 °C for 20 min and stopped with 10% SDS, followed by digestion with proteinase K and further incubated at 45 °C for 30 min. After the addition of the loading buffer, the reaction was heated for 2 min at 70 °C. Electrophoresis was carried out in a 1% agarose gel in TAE buffer containing 0.5 μg/mL ethidium bromide, and further the gel was destained with water for 20 min.

DNA Intercalation Assay. Using a plasmid mega kit (Zymo Research), negatively supercoiled plasmid was isolated from *E. coli*. The protocol followed was same as mentioned in the supplier manual. In this assay, 250 ng plasmid was incubated at 37 °C for 20 min with 1 μg/mL ethidium bromide, 100 μM standard drug (etoposide), or with the investigational compound. Samples were then loaded in 1% agarose gel and electrophoresis was carried out in TAE buffer. Further the gel was stained with ethidium bromide (0.5 μg/mL) for 15 min and destained with water for 20 min and photographed using BioRad.

Molecular Modeling. In the rational drug discovery pipeline, modeling and informatics play an indispensable role in the identification of lead compounds and their most plausible mechanisms of action against particular biological targets.[62] With this outlook, we have performed molecular modeling study on N-fused imidazole derivatives in order to identify their potential binding with the ATPase domain of hTopoIIα. To date, the structure of the complete hTopoIIα is unavailable and only the crystal structure of the ATPase domain of hTopoIIα has been reported.[50]

The 3D structure of the compounds under study were built using SYBYL 7.1 molecular modeling package,[49] installed on a Silicon Graphics Fuel Workstation running IRIX 6.5. Gasteiger−Hückel partial charges were applied to the atoms in the compound for geometry optimization. All the structures were then minimized by Powell method using Tripos force field, with 0.05 kcal/mol energy gradient convergence criterion. Finally, database of ligands was created in SYBYL.

Enzyme and Ligand Structure Preparation. The X-ray crystallographic structures of the ATPase domain of hTopoIIα (residues 29−428) bound to AMPPNP (5′-adenylyl-β,γ-imidodiphosphate, a nonhydrolyzable ATP analogue, PDB: 1ZXM) and ADP (PDB: 1ZXN), solved at 1.86 and 2.51 Å resolution respectively are available in the Protein Data Bank.[50] For the purpose of docking in the present work, the structure 1ZXM was selected because of its high resolution and better overall *B*-factor. 1ZXM is a homodimer consisting of two chains A and B, each having ligand AMPPNP and Mg ion in the ATP binding pocket. The Mg ion in an active site forms the distorted octahedral metal-ion coordination shell by making three point contacts with all three phosphates of AMPPNP, with the side chain carbonyl oxygen of Asn91 and two conserved water molecules (927 and 928).

Before enzyme structure preparation, chain A was extracted along with the associated AMPPNP and Mg ion, while chain B was removed. Enzyme structure was prepared by using the Protein Preparation Wizard tool implemented in Maestro interface (Maestro 9.0, Schrödinger, LLC, New York). The right bond orders were assigned, and the hydrogen atoms were added to the enzyme. The orientation of hydroxyl groups, amide groups of Asn and Gln, and charge state of His residues were optimized using the utility protassign. The final step was a restrained minimization by the impref utility until the average rmsd of the hydrogen atoms reached 0.3 Å, leaving heavy atoms in place. Magnesium ion was assigned a charge of +0.9.[30] Subsequently, two sets of prepared enzyme structure were saved, one after removing all the crystallographic water molecules and another with two conserved water molecules (927 and 928) in the active site while removing all others. Ligands were prepared using LigPrep module of Maestro interface by generating all possible low energy ionization, tautomeric, and stereoisomeric states within the range of pH 7.0 ± 2.0 using OPLS_2005 force field.

In the X-ray crystallographic structures of ATPase domain of hTopoIIα (PDB id: 1ZXM),[50] amino acid residues from 346 to 349 (loop region) and 406 to 428 (C-terminal) are missing in the chain A. For a successful dynamics run, it is necessary to add the missing residues of the loop region. Therefore, python script file defining the missing residues was run using Modeller9v8 program.[63] To obtain the complete amino acid sequence of ATPase domain of hTopoIIα, fasta format file was downloaded from UniProt (accession no. P11388). The fasta file was used as an input in the alignment script of Modeller9v8 and an alignment file was created. Subsequently, the python script file for adding missing residues was run and the three models with added

missing residues were generated from alignment information. The best model was selected on the basis of lowest MolPdf score and rmsd between the model and crystal structure.

Molecular Docking. In the previous molecular docking studies carried on ATPase domain of hTopoIIα to speculate the probable binding mode of synthesized compounds, some of the authors have considered water molecules in the active site of enzyme while performing docking simulation,[64] whereas other research groups have neglected the role of conserved water molecules.[29,30,58,65−67] Therefore, to understand the atomic level differences in terms of interactions, binding pose, and binding affinity of docked ligands in two cases, we have performed docking in two sets of prepared enzyme structure: with two conserved water molecules in the active site and without any water molecules. Docking simulation was performed by using three molecular docking programs FlexX,[48] GLIDE,[68] and GOLD.[69] The comparative docking results of FlexX, GLIDE, and GOLD molecular docking programs for some of the synthesized compounds and substrate ATP in presence and absence of two conserved water molecules in hTopoIIα ATP binding site are presented in Tables S1 and Table S2, respectively (see Supporting Information). The results reported in Tables S1 and S2 clearly indicate that FlexX scores can distinguish active/moderate/inactive ligands. Further, the poses and scores obtained using the two water molecules in the coordination mode with Mg ion were found to be more realistic. Hence, the results presented in this article are based on FlexX software, employing an enzyme structure with two water molecules included in the active site. FlexX program (version 1.2)[48] incorporated in SYBYL 7.1[49] by Tripos Associates was utilized for molecular docking. FlexX docking into the ATPase domain of hTopoIIα active site cavity consisted of three steps: (1) enzyme structure preparation, (2) constructing the ligand structure and building a ligand database for multiligand docking process, and (3) defining the receptor description file (RDF). RDF was generated in order to define the active site of the enzyme, using all residues located within 6.5 Å from a bound ligand (AMPPNP). FlexX is a technique for structure-based drug design based on an incremental construction method. Fragments of the ligand are automatically placed into the active site using an algorithmic approach based on a pattern recognition technique called pose clustering. Each pose of the ligand in the enzyme cavity is scored based on protein−ligand interactions. Finally, the binding energies are estimated in the form of docking score, poses are ranked, and the top ranking poses are chosen for analysis.

Initially, ATP and AMPPNP were docked into the ATPase domain of hTopoIIα. The rationale behind this docking was to validate the docking protocol by assessing the binding pose and hydrogen bonding interactions of these substrates with key residues of the ATPase domain of an enzyme. After successfully setting up the docking protocol and its validation, some of the synthesized compounds (potent, moderately active, and inactive) were docked, which were initially prepared in Maestro using LigPrep utility, while considering all possible tautomers of the species wherever possible. Docking simulations of these compounds were carried out using FlexX multiple ligand docking mode with a SYBYL database file as a ligand source. After running FlexX, 30 docked conformers were displayed in a molecular spread sheet and ranked according to their FlexX docking score. All the poses were visually inspected, and the most suitable docking pose was selected on the basis of score and interactions with Mg cation and key residues of the active site. Similar docking protocols were employed to perform molecular docking analyses using GLIDE and GOLD software (Supporting Information)

Molecular Dynamics Simulation. The best docking pose obtained from FlexX program for compound **5** of the series in complex with the enzyme structure with two conserved water molecules was saved as .pdb files for MD study. Full atomistic simulations were performed in water as an explicit solvent for enzyme−ligand complexes using AMBER 10[55] molecular dynamics software package.

From the enzyme−ligand complexes, ligand was extracted and saved as .mol2 file, which was further used as an input in the *Antechamber* module of AMBER to generate .prepin and .frcmod files. Partial atomic charges were calculated by AM1BCC method and charge on ligand molecule was set to −1. General Amber Force Field (GAFF) was used to generate missing parameters of the ligands. Parameters for Mg ion were taken from the parm99.dat file of AMBER.[70] The final processing of the enzyme−ligand complex was carried in *tleap* module of AMBER to generate parameter topology file of complex. Enzyme−ligand complexes were immersed in an octahedral water box using the TIP3P model[71] by choosing a 12 Å solvation shell around the complex structure. To neutralize the system, sufficient numbers of counter chloride ions were added. Afterward, coordinate (.inpcrd) and parameter (.prmtop) files of complex were generated.

The minimization of system was carried in three successive steps: In the first step, the enzyme−ligand complex was restrained with a force constant of 2 kcal/mol/Å^2 and only solvent phase was minimized with 500 cycles of each steepest descent and conjugate gradient methods. This allowed the water molecules to reorganize themselves to eliminate any bad contacts with the enzyme-ligand complex. In the second step, the restraint weight was reduced to 1 kcal/mol/Å^2 to maintain gradual decrease and 250 cycles minimization was implied as above. In the third step, the whole system was minimized for 500 cycles without putting any restraints by both minimization methods as mentioned above. The minimized complex structures were subjected to heating under NVT ensemble for 50 ps where the system was gradually heated from 0 to 310 K by putting restraint with a force constant of 2 kcal/mol/Å^2. Subsequently, 50 ps of density equilibration with weak restraints of 1 kcal/mol/Å^2 on the complex and 100 ps of density equilibration without any restraints followed by 500 ps of constant pressure equilibration at 310 K were performed.

Finally, production phase was performed under NPT ensemble at 310 K and 1 atm pressure for 1.3 ns. Equations of motion were solved using the Verlet leapfrog algorithm.[72] For entire simulation, the integration step size was taken as 2 fs, and the trajectory snapshots were saved after each 2 ps. During the MD run, all covalent bonds containing hydrogen atoms were constrained using SHAKE algorithm.[73] A Langevin thermostat and barostat was used for temperature and pressure coupling. The nonbonded cutoff was kept at 8 Å, and long-range electrostatic interactions were treated by the Particle-Mesh Ewald (PME) method. *Ptraj* module of Amber tools, VMD,[74] and Xmgrace were used for the analysis of trajectories. The trajectories obtained from MD were used for binding free energy calculations. The calculations were performed using MM-PBSA/GBSA method, implemented in Amber 10.[53,54]

ATPase Assay. ATP hydrolysis of hTopoIIα was evaluated by quantifying the inorganic phosphate which was released during the reaction. Six units of hTopoIIα and supercoiled plasmid DNA (pRYG) were combined in freshly prepared buffer (10 mM Tris-HCl, pH 7.5, 175 mM KCl, 0.1 mM EDTA, 5 mM $MgCl_2$, 2 mM DTT, 2.5% glycerol). Then compound **5** along with ATP was added to the reaction mixture and the resultant solution was incubated at 37 °C. After 20 min of incubation, reaction was stopped by the addition of malachite green reagent, and immediately OD was taken at 620 nm on microtiter plate reader (Thermo Scientific Multiskan Spectrum). For kinetic studies, same protocol was followed for increasing concentrations of ATP (200, 280, 360, 440, and 520 μM) at each respective fixed concentration of compound **5** (0, 50, 100, and 150 μM).

Cell Culture and Chemicals. The Vero (kidney epithelial cells of African green monkey), HEK 293 (Kidney cancer cells), and MCF 7 (Breast cancer cells) were maintained in Dulbecco's Modified Eagle's Medium (DMEM) with 1% antibiotic (100 units of penicillin and 10 mg streptomycin per mL in 0.9% normal saline) and 10% fetal bovine serum (Himedia, India) in a humidified CO_2 incubator in 5% CO_2 at 37 °C. The MCF 10A (normal breast epithelial cells) cells were grown in

DMEM/F-12 (50:50, v/v) medium supplemented with 10% (v/v) fetal bovine serum (Himedia, India), 100 U/mL of penicillin, 100 μg/mL streptomycin, 0.5 μg/mL of hydrocortisone, 100 ng/mL of cholera toxin, 10 μg/mL of insulin, 10 ng/mL of epidermal growth factor, and 1% (w/v) L-glutamine at 37 °C under a humidified CO_2 incubator in 5% CO_2 at 37 °C. 5-Fluorouracil, etoposide, and all other chemicals of analytical grade were purchased from Sigma Chemical Ltd. (St Louis, MO, USA). Stock solutions (100 mM) of investigational compounds were prepared in DMSO and stored at −20 °C. For treatment, the solution was diluted in DMEM and added to cultures to provide the desired final concentration. After 60−70% confluence, the cells were exposed to different compounds of indicated concentrations at required time periods.

Topoisomerase Inhibition Assay. Topoisomerase assay was used to assess the ability of compound **5** to inhibit the function of topoisomerase activity in conversion of negatively supercoiled plasmid DNA into relaxed/linear DNA.[75,76] As topoisomerases are nuclear proteins, we prepared nuclear cell lysate according to the protocol of Wiley Intersciences for preparation of mammalian cell nuclear extracts for assaying topoisomerase activity.[77] Confluent dishes (80−90%) were treated with either compound **5** of increasing concentrations or 100 μM etoposide (positive control) for 48 h prior to harvest, and then nuclear lysate was prepared. The topoisomerase reaction contains 100 μg nuclear protein, a common plasmid for substrate (FOP FLASH−TCF/LEF transcription factor, responsible for β−catenin-Wnt-signaling pathway) (1 μg) and reaction buffer (200 mM Tris-Cl, pH-7.5, 100 mM $MgCl_2$, 10 mM ATP, 10 mM EDTA, 10 mM dithiothreitol, 1.5 mM KCl, 300 μg/mL bovine serum albumin). The tubes were incubated at 37 °C for 30 min, and reaction was stopped by addition of 1% SDS. Then 30 μL of reaction mixture was loaded in each well of 0.9% horizontal agarose gel electrophoresis containing ethidium bromide. Electrophoresis was done for 3−4 h at 10−15 V. Photographs were taken using gel documentation system (UVP, Germany). Data presented here is the best of five experiments.

ATP Dependent Plasmid Relaxation Assay. To assess the ATP dependent topoisomerase activity of HEK 293 nuclear lysate, a plasmid based relaxation assay was carried out following the method as described above in topoisomerase inhibition assay. Instead of using compound **5** treated nuclear lysate, here compound **5** was added into the final reaction mixture. The reaction mixture contained 100 μg of protein, plasmid (FOP FLASH −TCF/LEF) (1 μg), 200 mM Tris-Cl, pH-7.5, 100 mM $MgCl_2$, 10 mM EDTA, 10 mM dithiothreitol, 1.5 mM KCl, 300 μg/mL bovine serum albumin, 35 μM compound **5**, and various concentrations of ATP (0, 20, 50, 100, 150, 200, 250 mM). Etoposide (100 μM) was used as positive control. Data presented here is the best of five experiments.

Clonogenic Cell Survival Assay. Exponentially growing HEK 293 cells were trypsinized and diluted to approximately 500−600 viable cells per well in 12-well culture plates. After 24 h of incubation, cells were treated with compounds of varying concentrations for 48 h. The media was aspirated and replaced with fresh normal growth medium, and cells were allowed to grow for 5−6 doubling.[78] Media was removed and plates were air-dried. Colonies were stained with 0.2% crystal violet for 1 h. The excess dye was repeatedly washed with distilled water. Plates were air-dried, and stained colonies were manually counted. The data presented is percent survival with respect to control and is the best of three independent experiments.

MTT Cell Survival Assay. Survival of the cells after treatment with drug was measured using 3-(4,5-dimethylthiazol-2-yl)-2,5-diphenyltetrazolium bromide (MTT) cell survival assay. Briefly, 8000−10000 cells of HEK 293, Vero, MCF 7, and MCF 10A were plated in triplicate in different 96-well flat-bottom tissue culture plates, and after 24 h of seeding, they were exposed to either investigational compounds or etoposide of different concentrations for 48 h. For time scan analysis, the cells were treated with 12 μM of compound **5** at different time periods. After completion of treatment, the media was removed, 100 μL of 0.05% MTT reagent was added to each well, and it was incubated at 37 °C for overnight to allow the formation of purple formazan crystals. A 100 μL of NP-40 detergent solution was added to each well, and the reaction mixture was incubated in dark for 1 h at room temperature for dissolving the formazan crystals. Color density was measured spectrophotometrically at 570 nm using microplate reader (Berthold, Germany). Experiments were conducted in triplicates, and the data is presented as percent survival.

Wound Healing Assay. HEK 293 cells were cultured in 35 mm tissue culture discs to 90% confluence. A sterile micro tip was used to create a clean wound in the cell mono layer across the center of the well. Cell debris was removed by washing the plates with fresh media. The cells were exposed to compound **5** (0, 15, 25, and 35 μM) and were allowed to migrate in the medium. The wound was assessed by a microscope (Nikon, Japan) at 10× magnification at different time point (0, 6, 12, and 24 h).

DAPI Staining. Roughly 1×10^6 HEK 293 cells were seeded in 35 mm tissue culture discs. Cells were treated with compound **5** of increasing concentrations (0, 15, 25, and 35 μM) for 48 h. After treatment, the cells were fixed with ice chilled acetone:methanol (1:1) for 30 min at 4 °C in dark. Fixed cells were washed twice with chilled 1× PBS, and then stained with DAPI for 1 h at 4 °C in dark. Stained cells were washed repeatedly with chilled 1× PBS to remove the excess DAPI stain and observed under fluorescence microscope (Nikon, Japan) at 40× magnification.

FACS Analysis. HEK 293 cells (1×10^6) were cultured in 60 mm tissue culture plates. After 70−80% confluence, cells were exposed to different concentrations (0, 15, 25, and 35 μM) of compound **5** for 48 h. After treatment, cells were trypsinized and washed twice with 1× PBS containing 0.05% RNase-A. Finally, cells were resuspended in 0.1 mL of propidium iodide solution (50 μg/mL). Cells were incubated for 30 min in dark at room temperature. Fluorescence emitted from propidium iodide−DNA complexes was quantified after laser excitation of the fluorescent dye by Fluorescence-Activated Cell Sorter (FACS) (Becton and Dickinson, CA). Finally, DNA content of the cells at different phases of cell cycle was determined by using Cell Quest Software (Becton and Dickinson, CA).

SDS-PAGE and Western Blot Analysis. HEK 293 cells were grown on 100 mm tissue culture discs at a density of 1×10^6 cells per plate and incubated overnight. Then the cells were exposed to compound **5** (0, 15, 25, and 35 μM) for 48 h prior to harvest. The cell lysate was prepared by using modified RIPA lysis buffer (50 mM tris, 150 mM NaCl, 0.5 mM deoxycholate, 1% NP-40, 0.1% SDS, 1 mM Na_3VO_4, 5 mM EDTA, 1 mM PMSF, 2 mM DTT, 10 mM β-glycerophosphate, 50 mM NAF, 0.5% triton X-100, protease inhibitor cocktail). Protein estimation was done by Bradford's method. Proteins were separated in 10% SDS-PAGE and transferred to PVDF membrane. Membranes were blocked overnight in 10% skimmed milk in 1× TBS-T (Tris-buffered saline containing 0.05% of Tween-20) at 4 °C and immunoblotted with antibodies anti-Bcl-XL, anti-Bax, and anti-PARP. Detection of signals was done using ECL Western blotting reagent and chemiluminescence was exposed on Kodak X-Omat films. Antibody anti-β-actin was used as loading control. All the antibodies were procured from cell signaling technology, CA, USA.

Statistical Analysis. A two-tailed Student's *t* test was employed where $P < 0.05$ was considered to be statistically significant.

■ ASSOCIATED CONTENT

Supporting Information. General experimental procedure; ^1H, ^{13}C, mass, IR, CHN, or HRMS, and melting points for all compounds, determination of LC_{50} value of compound **5** for

hTopoIIα-decatenation in vitro assay, molecular docking protocols for GLIDE and GOLD, tautomeric preferences and MD simulation analysis. This material is available free of charge via the Internet at http://pubs.acs.org.

AUTHOR INFORMATION

Corresponding Author

*For S.K.G.: phone, +91 (0)172 2214683; fax, +91 (0)172 2214692; E-mail, skguchhait@niper.ac.in. For C.N.K.: phone, +91 (0)674 2725466; fax, + 91 (0)674 2725732; E-mail, cnkundu@gmail.com.

ACKNOWLEDGMENT

We gratefully acknowledge the financial support from DST, ICMR, and DBT, Government of India, New Delhi, for this investigation. We are thankful to Antara Chakraborty for her assistance in some of the experiments of cancer cell lines.

ABBREVIATIONS USED

hTopoIIα Human topoisomerase IIα; MDR multidrug resistance; MCR multicomponent reaction; kDNA kinetoplast DNA; Nck nicked; Rel relaxed; SC supercoiled; Lin linear; AMPPNP 5′-adenylyl-β,γ-imidodiphosphate; rmsd root-mean-square deviation; MD molecular dynamics; MM-PBSA molecular mechanics Poisson—Boltzmann surface area; MM-GBSA molecular mechanics generalized Born surface area; FACS fluorescence activated cell sorter; DAPI 4′-6-diamidino-2-phenylindole; NCEs new chemical entities; RDF receptor description file; TAE Tris-acetate-EDTA; DMEM Dulbecco's Modified Eagle's Medium; MTT 3-(4,5-dimethylthiazol-2-yl)-2,5-diphenylte-trazolium bromide

REFERENCES

(1) Andoh,T., Ed. *DNA Topoisomerases in Cancer Therapy: Present and Future*; Kluwer Academic/Plenum: New York, 2003.

(2) Nitiss, J. L. Targeting DNA topoisomerase II in cancer chemotherapy. *Nature Rev. Cancer* **2009**, *9*, 338–350.

(3) Wang, H. K.; Morris-Natschke, S. L.; Lee, K. H. Recent advances in the discovery and development of topoisomerase inhibitors as antitumor agents. *Med. Res. Rev.* **1997**, *17*, 367–425.

(4) Haglof, K. J.; Popa, E.; Hochster, H. S. Recent developments in the clinical activity of topoisomerase-I inhibitors. *Update Cancer Ther.* **2006**, *1*, 117–145.

(5) Pommier, Y. DNA topoisomerase I inhibitors: chemistry, biology, and interfacial inhibition. *Chem. Rev.* **2009**, *109*, 2894–2902.

(6) Hande, K. R. Clinical applications of anticancer drugs targeted to topoisomerase II. *Biochim. Biophys. Acta* **1998**, *1400*, 173–184.

(7) Hande, K. R. Etoposide: four decades of development of a topoisomerase II. *Eur. J. Cancer* **1998**, *34*, 1514–1521.

(8) Zunino, F.; Capranico, G. DNA topoisomerase II as the primary target of anti-tumor anthracyclines. *Anti-Cancer Drug Discovery* **1990**, *5*, 307–317.

(9) Nitiss, J. L.; Liu, Y. X.; Harbury, P.; Jannatipour, M.; Wasserman, R.; Wang, J. C. Amsacrine and etoposide hypersensitivity of yeast cells overexpressing DNA topoisomerase II. *Cancer Res.* **1992**, *52*, 4467–4472.

(10) Pommier, Y. Topoisomerase I inhibitors: camptothecins and beyond. *Nature Rev. Cancer* **2006**, *6*, 789–802.

(11) Thomas, C. J.; Rahier, N. J.; Hecht, S. M. Camptothecin: current perspectives. *Bioorg. Med. Chem.* **2004**, *12*, 1585–1604.

(12) Salerno, S.; Da Settimo, F.; Taliani, S.; Simorini, F.; La Motta, C.; Fornaciari, G.; Marini, A. M. Recent advances in the development of dual topoisomerase I and II inhibitors as anticancer drugs. *Curr. Med. Chem.* **2010**, *17*, 4270–4290.

(13) Wang, J. C. Cellular roles of DNA topoisomerases: a molecular perspective. *Nature Rev. Mol. Cell Biol.* **2002**, *3*, 430–440.

(14) Nitiss, J. L. DNA topoisomerase II and its growing repertoire of biological functions. *Nature Rev. Cancer* **2009**, *9*, 327–337.

(15) Champoux, J. J. DNA topoisomerase: structure, function, and mechanism. *Annu. Rev. Biochem.* **2001**, *70*, 369–413.

(16) Goto, T.; Wang, J. C. Yeast DNA topoisomerase II: an ATP-dependent type II topoisomerase that catalyzes the catenation, decatenation, unknotting, and relaxation of double-stranded DNA rings. *J. Biol. Chem.* **1982**, *257*, 5866–5872.

(17) Stewart, L.; Redinbo, M. R.; Qiu, X.; Hol, W. G. J.; Champoux, J. J. A model for the mechanism of human topoisomerase I. *Science* **1998**, *279*, 1534–1541.

(18) Li, Y. Y. Some nonlinear elliptic equations from geometry. *Proc. Natl. Acad. Sci. U.S.A.* **2002**, *99*, 15287–15290.

(19) Brown, P. O.; Cozzarelli, N. R. A sign inversion mechanism for enzymatic supercoiling of DNA. *Science* **1979**, *206*, 1081–1083.

(20) Woessner, R. D.; Mattern, M. R.; Mirabelli, C. K.; Johnson, R. K.; Drake, F. H. Proliferation- and cell cycle-dependent differences in expression of the 170 kDa and 180 kDa forms of topoisomerase II in NIH-3T3 cells. *Cell Growth Differ.* **1991**, *2*, 209–214.

(21) Issacs, R. J.; Davies, S. L.; Sandri, M. I.; Redwood, C.; Wells, N. J.; Hickson, I. D. Physiological regulation of eukaryotic topoisomerase II. *Biochim. Biophys. Acta* **1998**, *1400*, 121–137.

(22) Bromberg, K. D.; Burgin, A. B.; Osheroff, N. A. A two-drug model for etoposide action against human topoisomerase II alpha. *J. Biol. Chem.* **2003**, *278*, 7406–7412.

(23) Austin, C. A.; Marsh, K. L. Eukaryotic DNA topoisomerase II β. *BioEssays* **1998**, *20*, 215–226.

(24) Gatto, B.; Leo, E. Drugs acting on the beta isoform of human topoisomerase II. *Curr. Med. Chem. Anti-Cancer Agents* **2003**, *3*, 175–185.

(25) Hande, K. R. Topoisomerase II inhibitors. *Update Cancer Ther.* **2008**, *3*, 13–26.

(26) McClendon, A. K.; Osheroff, N. DNA topoisomerase II, genotoxicity, and cancer. *Mutat. Res.* **2007**, *623*, 83–97.

(27) Winick, N. J.; McKenna, R. W.; Shuster, J. J.; Schneider, N. R.; Borowitz, M. J.; Bowman, W. P.; Jacaruso, D.; Kamen, B. A.; Buchanan, G. R. Secondary acute myeloid leukemia in children with acute lymphoblastic leukemia treated with etoposide. *J. Clin. Oncol.* **1993**, *11*, 209–217.

(28) Larsen, A. K.; Escargueil, A. E.; Skladanowski, A. Catalytic topoisomerase II inhibitors in cancer therapy. *Pharmacol. Ther.* **2003**, *99*, 167–181.

(29) Huang, H.; Chen, Q.; Ku, X.; Meng, L.; Lin, L.; Wang, X.; Zhu, C.; Wang, Y.; Chen, Z.; Li, M.; Jiang, H.; Chen, K.; Ding, J.; Liu, H. A series of α-heterocyclic carboxaldehyde thiosemicarbazones inhibit topoisomerase IIα catalytic activity. *J. Med. Chem.* **2010**, *53*, 3048–3064.

(30) Jiménez-Alonso, S.; Orellana, H. C.; Braun, A. E.; Ravelo, A. G.; Sacau, E. P.; Machín, F. Design and synthesis of a novel series of pyranonaphthoquinones as topoisomerase II catalytic inhibitors. *J. Med. Chem.* **2008**, *51*, 6761–6772.

(31) Yoshida, M.; Maehara, Y.; Sugimachi, K. MST-16, a novel bis-dioxopiperazine anticancer agent, ameliorates doxorubicin-induced acute toxicity while maintaining antitumor efficacy. *Clin. Cancer Res.* **1999**, *5*, 4295–4300.

(32) Weiss, G.; Loyevsky, M.; Gordeuk, V. R. Dexrazoxane (ICRF-187). *Gen. Pharm.* **1999**, *32*, 155–158.

(33) Lang, J. Y.; Chen, H.; Zhou, J.; Zhang, X. W.; Li, M. H.; Lin, L. P.; Zhang, J. S.; Waalkes, M. P.; Ding, J. Antimetastatic effect of salvicine on human breast cancer MDA-MB-435 orthotopic xenograft is closely related to Rho-dependent pathway. *Clin. Cancer Res.* **2005**, *11*, 3455–3464.

(34) Mashimo, T.; Bandyopadhyay, S.; Goodarzi, G.; Watabe, M.; Pai, S. K.; Gross, S. C.; Watabe, K. Activation of tumor metastasis suppressor gene, KA11, by etoposide is mediated by P53 and C-Jun genes. *Biochem. Biophys. Res. Commun.* **2000**, *274*, 370–376.

(35) Chang, X.; Tou, J. C.; Hong, C.; Kim, H. A.; Riby, J. E.; Firestone, G. L.; Bjeldanes, L. F. 3,3′-Diindolylmethane inhibits angiogenesis and the growth of transplantable human breast carcinoma in athymic mice. *Carcinogenesis* **2005**, *26*, 771–778.

(36) Chow, K. C.; Macdonald, T. L.; Ross, W. E. DNA Binding by epipodophylotoxins and *N*-acyl anthracyclins: implications of mechanism of topoisomerase II inhibition. *Mol. Pharmacol.* **1988**, *34*, 67–473.

(37) Pinar, A.; Yurdakul, P.; Ylildiz, I.; Temiz-Arpaci, O.; Acan, N. L.; Aki-Sener, E.; Yalcin, I. Some fused heterocyclic compounds as eukaryotic topoisomerase II inhibitors. *Biochem. Biophys. Res. Commun.* **2004**, *317*, 670–674.

(38) Tekiner-Gulbas, B.; Temiz-Arpaci, O.; Yildiz, I.; Aki-Sener, E.; Yalcin, I. 3D-QSAR study on heterocyclic topoisomerase II inhibitors using CoMSIA. *SAR QSAR Environ. Res.* **2006**, *17*, 121–132.

(39) Chernyak, D.; Chernyak, N.; Gevorgyan, V. General and efficient Cu-catalyzed three component coupling reaction toward imidazoheterocycles: one-pot synthesis of alpidem and zolpidem. *Angew. Chem., Int. Ed.* **2010**, *49*, 2743–2746.

(40) Jin, Y.; Rho, M.-C.; Gajulapati, K.; Jung, H. Y.; Boovanahalli, S. K; Lee, J. H.; Song, G.-Y.; Choi, J. H.; Kim, Y. K.; Lee, K.; Choi, Y. Synthesis of a novel series of imidazo[1,2-α]pyridines as acyl-CoA: cholesterol acyltransferase (ACAT) inhibitors. *Bull. Korean Chem. Soc.* **2009**, *30*, 1297–1304.

(41) Guchhait, S. K.; Kundu C. N.; Banerjee, U. C.; Baviskar, A.; Madaan, C.; Agarwal A.; Preet, R.; Mohapatra, P. N-Fused aminoimidazoles as novel topoisomerase IIα-targeting anticancer agents. Indian Patent, application no. 91/DEL/2011, 2011.

(42) Guchhait, S. K.; Jadeja, K.; Madaan, C. A new process of multicomponent povarov reaction-aerobic dehydrogenation: synthesis of polysubstituted quinolines. *Tetrahedron Lett.* **2009**, *50*, 6861–6865.

(43) Guchhait, S. K.; Madaan, C. An efficient regioselective versatile synthesis of N-fused 2- and 3-aminoimidazoles via ugitype multicomponent reaction mediated by zirconium(IV) chloride in polyethylene glycol-400. *Synlett* **2009**, 628–632.

(44) Guchhait, S. K.; Madaan, C.; Thakkar, B. S. A highly flexible and efficient Ugi-type multicomponent synthesis of versatile N-fused aminoimidazoles. *Synthesis* **2009**, 3293–3300.

(45) Guchhait, S. K.; Madaan, C. Towards molecular diversity: dealkylation of *tert*-butyl amine in Ugi-type multicomponent reaction product establishes *tert*-butyl isocyanide as a useful convertible isonitrile. *Org. Biomol. Chem.* **2010**, *8*, 3631–3634.

(46) Besterman, J. M.; Elwell, L. P.; Cragoe, E. J.; Andrews, C. W.; Cory, M. DNA intercalation and inhibition of topoisomerase II. *J. Biol. Chem.* **1989**, *265*, 2324–2330.

(47) Burres, N. S.; Sazesh, S.; Gunawardana, G. P.; Clement, J. J. Antitumor activity and nucleic acid binding properties of dercitin, a new acridine alkaloid isolated from a marine dercitus species sponge. *Cancer Res.* **1989**, *49*, 5267–5274.

(48) Rarey, M.; Kramer, B.; Lengauer, T.; Klebe, G. A fast flexible docking method using an incremental construction algorithm. *J. Mol. Biol.* **1996**, *261*, 470–489.

(49) *SYBYL 7.1*; Tripos Inc.: St. Louis, MO 63144.

(50) Wei, H.; Ruthenburg, A. J.; Bechis, S. K.; Verdine, G. L. Nucleotide-dependent domain movement in the ATPase domain of a human type IIA DNA topoisomerase. *J. Biol. Chem.* **2005**, *280*, 37041–37047.

(51) Walker, J. E.; Saraste, M.; Runswick, M. J.; Gay, N. J. Distantly related sequences in the alpha- and beta-subunits of ATP synthase, myosin, kinases and other ATP-requiring enzymes and a common nucleotide binding fold. *EMBO J.* **1982**, *1*, 945–951.

(52) Wessel, I.; Jensen, L. H.; Jensen, P. B.; Falck, J.; Rose, A.; Roerth, M.; Nitiss, J. L.; Sehested, M. Human small cell lung cancer NYH cells selected for resistance to the bisdioxopiperazine topoisomerase II catalytic inhibitor ICRF-187 demonstrate a functional R162Q mutation in the walker a consensus ATP binding domain of the alpha isoform. *Cancer Res.* **1999**, *59*, 3442–3450.

(53) Wessel, I.; Jensen, L. H.; Renodon-Corniere, A.; Sorensen, T. K.; Nitiss, J. L.; Jensen, P. B.; Sehested, M. Human small cell lung cancer NYH cells resistant to the bisdioxopiperazine ICRF-187 exhibit a functional dominant Tyr165Ser mutation in the Walker A ATP binding site of topoisomerase IIα. *FEBS Lett.* **2002**, *520*, 161–166.

(54) Skouboe, C.; Bjergbaek, L.; Oestergaard, V. H.; Larsen, M. K.; Knudsen, B. R.; Andersen, A. H. A human topoisomerase IIα heterodimer with only one ATP binding site can go through successive catalytic cycles. *J. Biol. Chem.* **2003**, *278*, 5768–5774.

(55) Case, D. A.; Darden, T. A.; Cheatham, T. E., III; Simmerling, C. L.; Wang, J.; Duke, R. E.; Luo, R.; Crowley, M.; Walker, R. C.; Zhang, W.; Merz, K. M.; Wang, B.; Hayik, S.; Roitberg, A.; Seabra, G.; Kolossváry, I.; Wong, K. F.; Paesani, F.; Wu, X.; Brozell, S.; Steinbrecher, T.; Gohlke, H.; Yang, L.; Tan, C.; Mongan, J.; Hornack, V.; Cui, G.; Mathews, D. H.; Seetin, M. G.; Sagui, C.; Babin, V.; Kollman, P. A. *AMBER 10*; University of California, San Francisco, 2008.

(56) Srinivasan, J.; Cheatham, T. E.; Cieplak, P.; Kollman, P. A.; David, A. Continuum solvent studies of the stability of DNA, RNA, and phosphoramidate-DNA helices. *J. Am. Chem. Soc.* **1998**, *120*, 9401–9409.

(57) Ghosh, A.; Rapp, C. S.; Friesner, R. A. Generalized Born model based on a surface integral formulation. *J. Phys. Chem. B* **1998**, *102*, 10983–10990.

(58) Wang, P.; Leung, C.-H.; Ma, D.-L.; Lu, W.; Che, C.-M. Organoplatinum(II) complexes with nucleobase motifs as inhibitors of human topoisomerase II catalytic activity. *Chem.—Asian J.* **2010**, *5*, 2271–2280.

(59) Chène, P.; Rudloff, J.; Schoepfer, J.; Furet, P.; Meier, P.; Qian, Z.; Schlaeppi, J.-M.; Schmitz, R.; Radimerski, T. Catalytic inhibition of topoisomerase II by a novel rationally designed ATP-competitive purine analogue. *BMC Chem. Biol.* **2009**, *9*, 1.

(60) Kundu, C. N.; Balusu, R.; Jaiswal, A. S.; Gairola, C. G.; Narayan, S. Cigarette smoke condensate-induced level of adenomatous polyposis coli blocks long-patchbase excision repair in breast epithelial cells. *Oncogene* **2007**, *26*, 1428–1438.

(61) Sasaki, K.; Tsuno, N. H.; Sunami, E.; Tsurita, G.; Kawai, K.; Okaji, Y.; Nishikawa, T.; Shuno, Y.; Hongo, K.; Hiyoshi, M.; Kaneko, M.; Kitayama, J.; Takahashi, K.; Nagawa, H. Chloroquine potentiates the anti-cancer effect of 5-fluorouracil on colon cancer cells. *BMC Cancer* **2010**, *10*, 370.

(62) Bharatam, P. V.; Khanna, S.; Francis, S. M. Modeling and informatics in drug design. In *Preclinical Development Handbook: ADME and Biopharmaceutical Properties*; Cox, G. A. D., Ed.; John Wiley & Sons, Inc.: Hoboken, NJ, 2008; pp 1−45.

(63) Martí-Renom, M. A.; Stuart, A. C.; Fiser, A.; Sánchez, R.; Melo, F.; Šali, A. Comparative protein structure modeling of genes and genomes. *Annu. Rev. Biophys. Biomol. Struct.* **2000**, *29*, 291–325.

(64) Furet, P.; Schoepfer, J.; Radimerski, T.; Chéne, P. Discovery of a new class of catalytic topoisomerase II inhibitors targeting the ATP-binding site by structure based design. Part I. *Bioorg. Med. Chem. Lett.* **2009**, *19*, 4014–4017.

(65) Qin, Y.; Meng, L.; Hu, C.; Duan, W.; Zuo, Z.; Lin, L.; Zhang, X.; Ding, J. Gambogic acid inhibits the catalytic activity of human topoisomerase II by binding to its ATPase domain. *Mol. Cancer Ther.* **2007**, *6*, 2429–2440.

(66) Jun, K. Y.; Lee, E. Y.; Jung, M. J.; Lee, O. H.; Lee, E. S.; Park Choo, H. Y.; Na, Y.; Kwon, Y. Synthesis, biological evaluation, and molecular docking study of 3-(3′-heteroatom substituted-2′-hydroxy-1′-propyloxy) xanthone analogues as novel topoisomerase IIα catalytic inhibitor. *Eur. J. Med. Chem.* **2011**, *46*, 1964–1971.

(67) Gui, M.; Shi, D. K.; Huang, M.; Zhao, Y.; Sun, Q. M.; Zhang, J.; Chen, Q.; Feng, J. M.; Liu, C. H.; Li, M.; Li, Y. X.; Geng, M.; Ding, J. D11, a novel glycosylated diphyllin derivative, exhibits potent anticancer activity by targeting topoisomerase IIα. *Invest. New Drugs* **2010**, DOI: 10.1007/S10637-010-9425-9431.

(68) *Glide, version 5.5*; Schrödinger, LLC: New York, 2009.

(69) Jones, G.; Willett, P.; Glen, R. C.; Leach, A. R.; Taylor, R. Development and validation of a genetic algorithm for flexible docking. *J. Mol. Biol.* **1997**, *267*, 727–748.

(70) Aaqvist, J. Ion−water interaction potentials derived from free energy perturbation simulations. *J. Phys. Chem.* **1990**, *94*, 8021–8024.

(71) Jorgensen, W. L.; Chandrasekhar, J.; Madura, J. D.; Impey, R. W.; Klein, M. L. Comparison of simple potential functions for simulating liquid water. *J. Chem. Phys.* **1983**, *79*, 926–935.

(72) Verlet, L. Computer "experiments" on classical fluids. I. Thermodynamical properties of Lennard-Jones molecules. *Phys. Rev.* **1967**, *159*, 98–103.

(73) Ryckaert, J.-P.; Ciccotti, G.; Berendsen, H. J. C. Numerical integration of the Cartesian equations of motion of a system with constraints: molecular dynamics of *n*-alkanes. *J. Comput. Phys.* **1977**, *23*, 327–341.

(74) Humphrey, W.; Dalke, A.; Schulten, K. VMD—Visual Molecular Dynamics. *J. Mol. Graphics* **1996**, *14*, 33–38.

(75) Goodell, J. R.; Ougolkov, A. V.; Hiasa, H.; Kaur, H.; Remmel, R.; Billadeau, D. D.; Ferguson, D. M. Acridine-based agents with topoisomerase II activity inhibit pancreatic cancer cell proliferation and induce apoptosis. *J. Med. Chem.* **2008**, *51*, 179–182.

(76) Opperard, L. M.; Ougolkov, A. V.; Luchini, D. N.; Schoon, R. A.; Goodell, J. R.; Kaur, H.; Billadeau, D. D.; Ferguson, D. M.; Hiasa, H. Novel acridine-based compounds that exhibit an anti-pancreatic cancer activity are catalytic inhibitors of human topoisomerase II. *Eur. J. Pharmacol.* **2009**, *602*, 223–229.

(77) Halligan, B. D.; Edwards, K.; Liu, L. F. Purification and characterization of a type II DNA topoisomerase from bovine calf thymus. *J. Biol. Chem.* **1985**, *260*, 2475–2482.

(78) Jani, T, S.; DeVecchio, J.; Mazumdar, T.; Agyeman, A.; Houghton, J. A. Inhibition of NF-κB signaling by quinacrine is cytotoxic to human colon carcinoma cell lines and is synergistic in combination with tumor necrosis factor-related apoptosis-inducing ligand (TRAIL) or oxaliplatin. *J. Biol. Chem.* **2010**, *285*, 19162–19172.